Peculiar velocities

Model linear peculiar velocity field projected on the super-Galactic plane

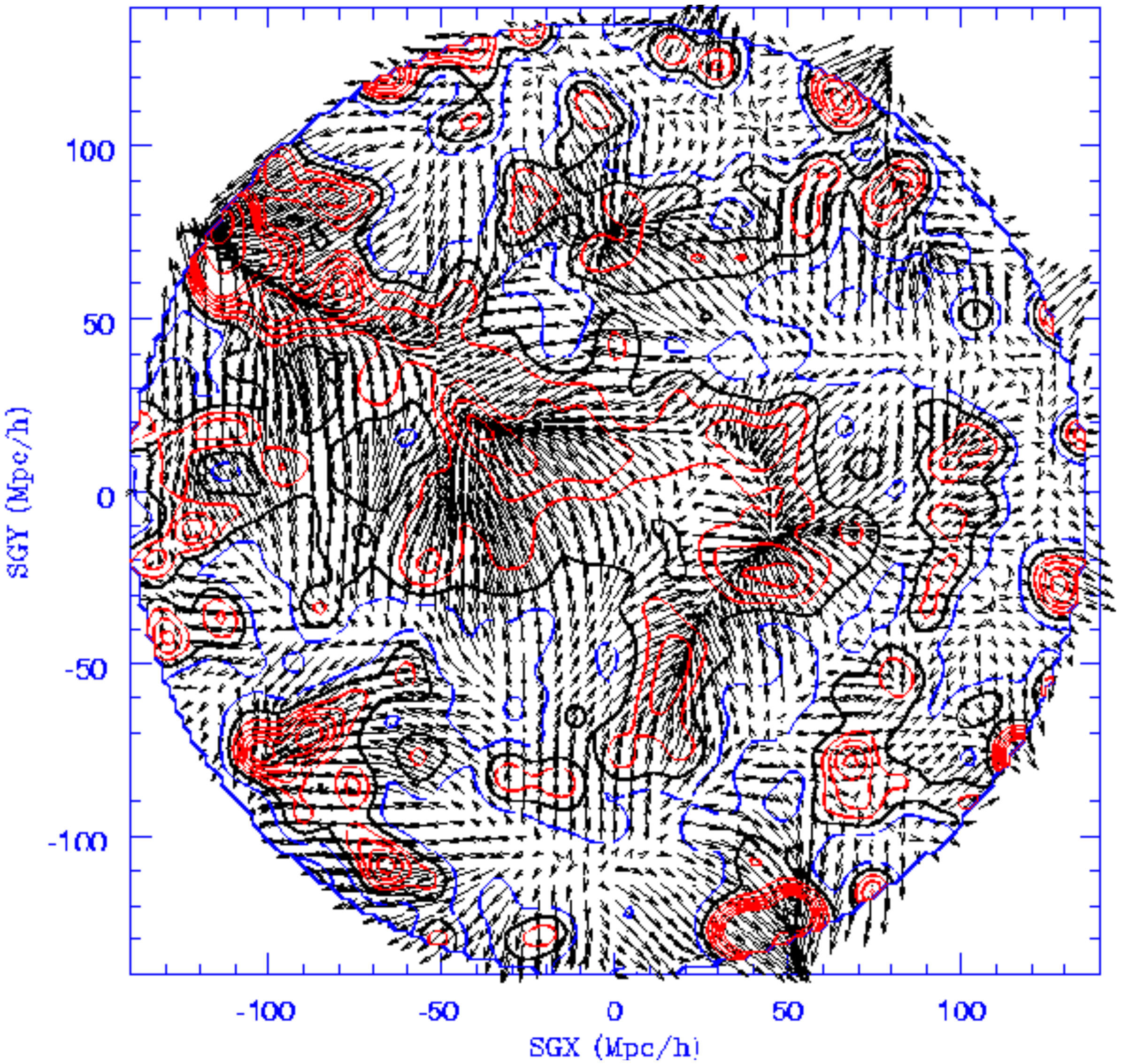

PECULIAR VELOCITIES

As a result, using the redshift as distance proxy induces ”redshift space distortions”, RSD, in the mapped 3D distribution of galaxies.

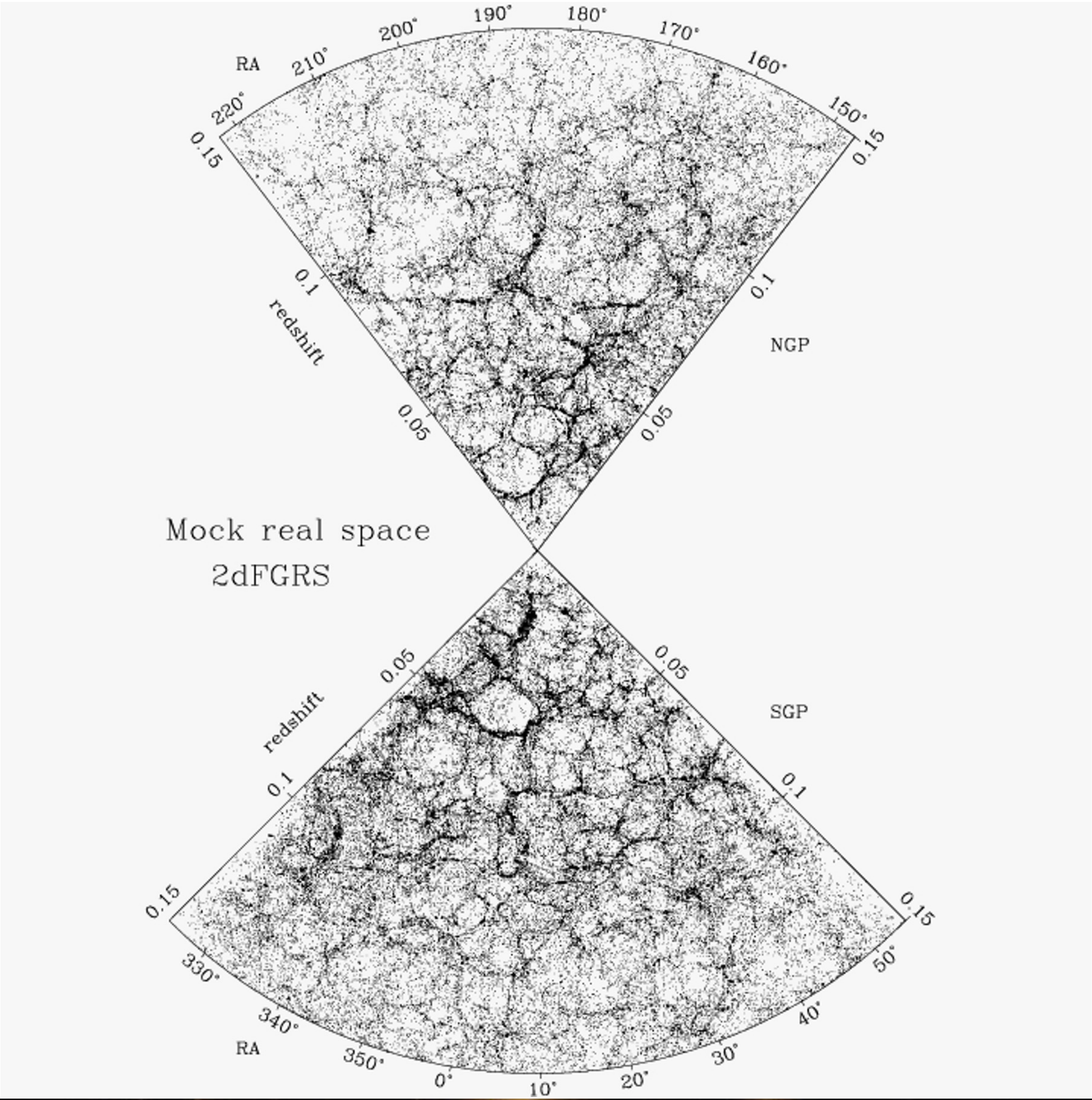

Peculiar velocities

As a result, using the redshift as distance proxy induces ”redshift space distortions”, RSD, in the mapped 3D distribution of galaxies.

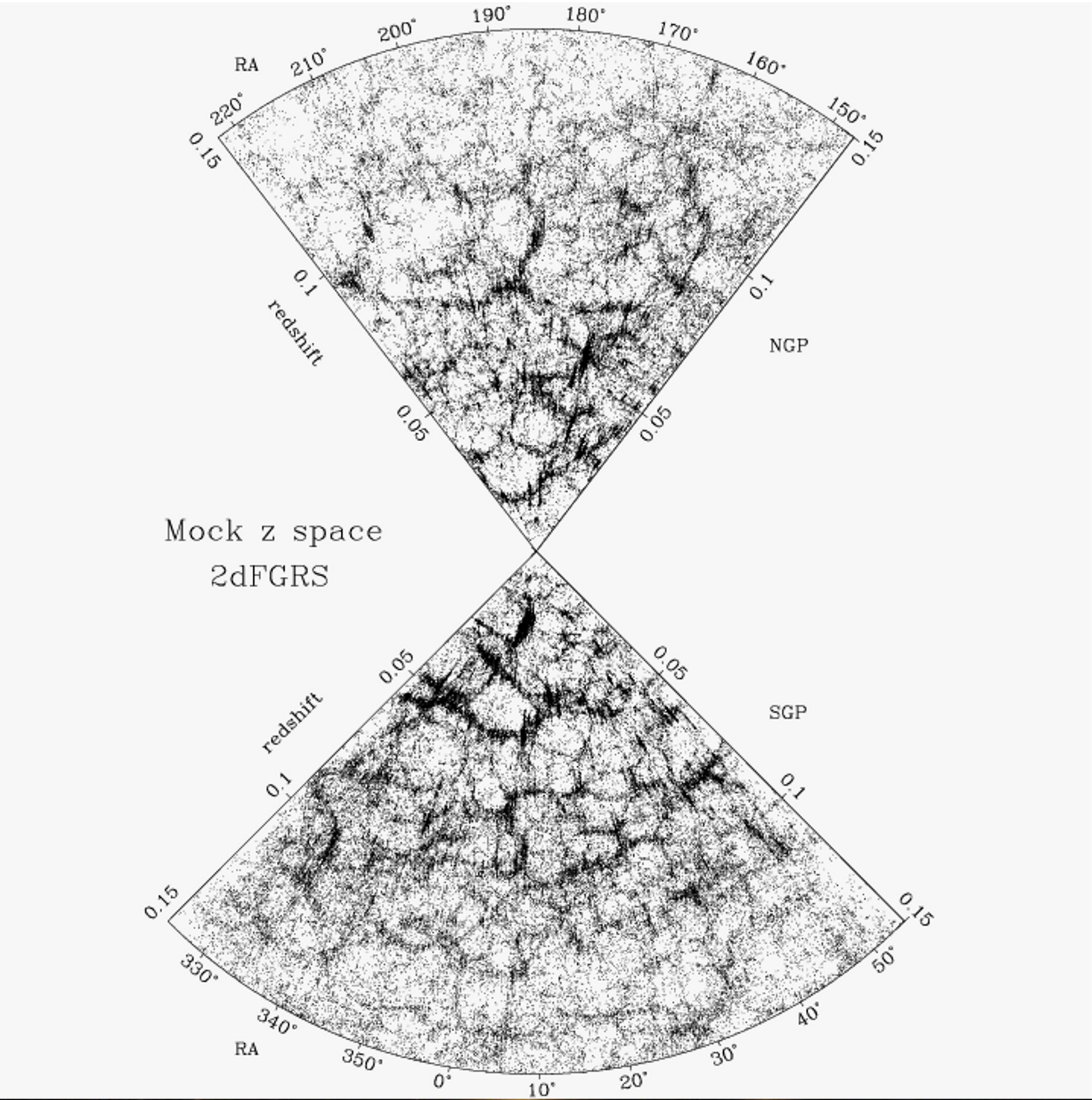

Peculiar velocities

We can qualitatively assess the impact of RSD on the 2PCF.

Let us consider the two components, parallel and perpendicular to the line of sight, of the pair separation vector $\boldsymbol{r} = (r_p, \pi)$ and tabulate pair counts accordingly.
The resulting 2D 2-point correlation $\xi = (r_p, \pi)$ will not be distorted along r_p. Just along the line of sight direction π.
The amplitude of these distortions is proportional to that of peculiar velocities, i.e. to the linear growth rate f.

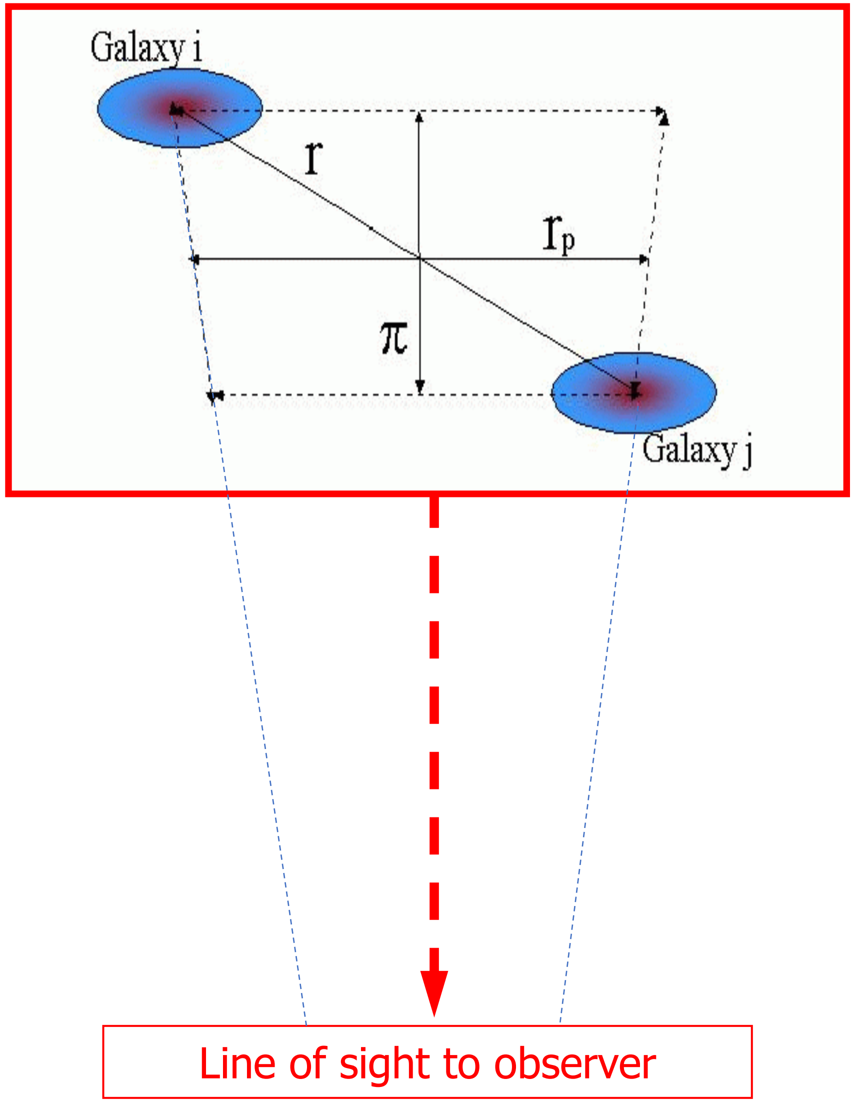

Peculiar velocities

With no peculiar velocities the iso-correlation contours are circular.

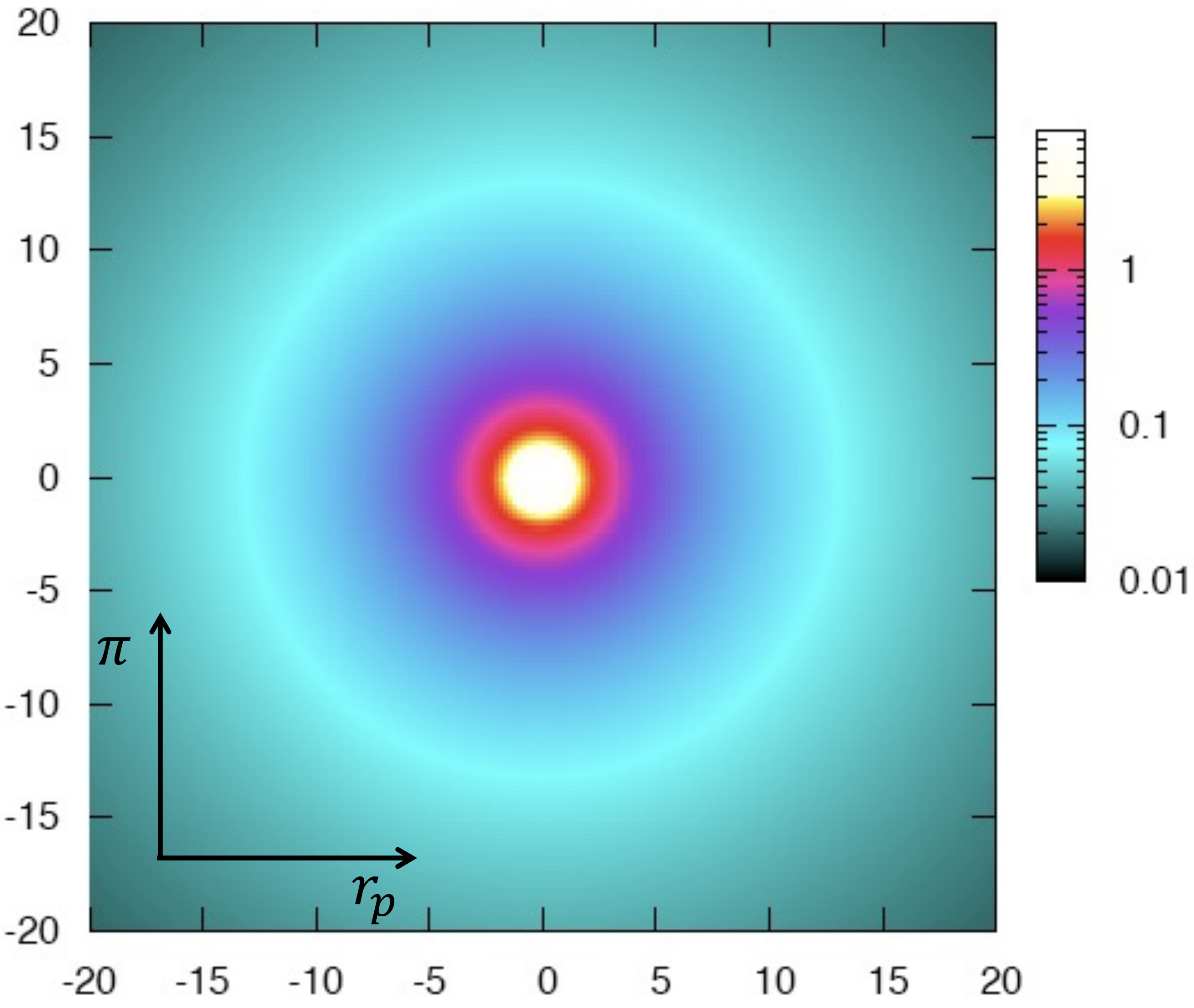

Peculiar velocities

Coherent linear velocities induce distortions along the line of sight that increase the apparent clustering signal. As a result, correlation contours squeeze along the line of sight direction.

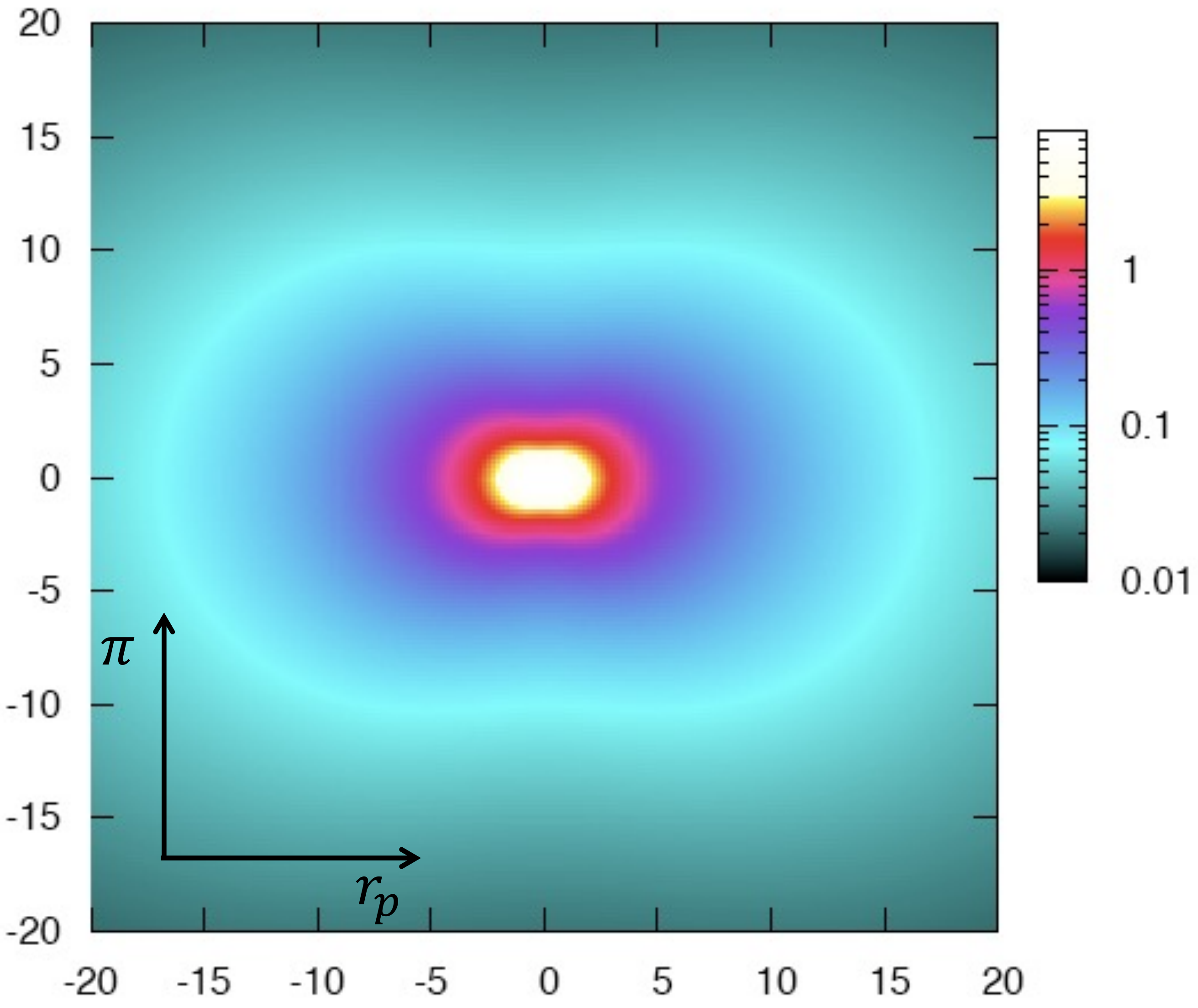

Peculiar velocities

Incoherent peculiar velocities induce different distortions along the line of sight. These reduce the apparent clustering signal along π but only for pairs with small r_p.

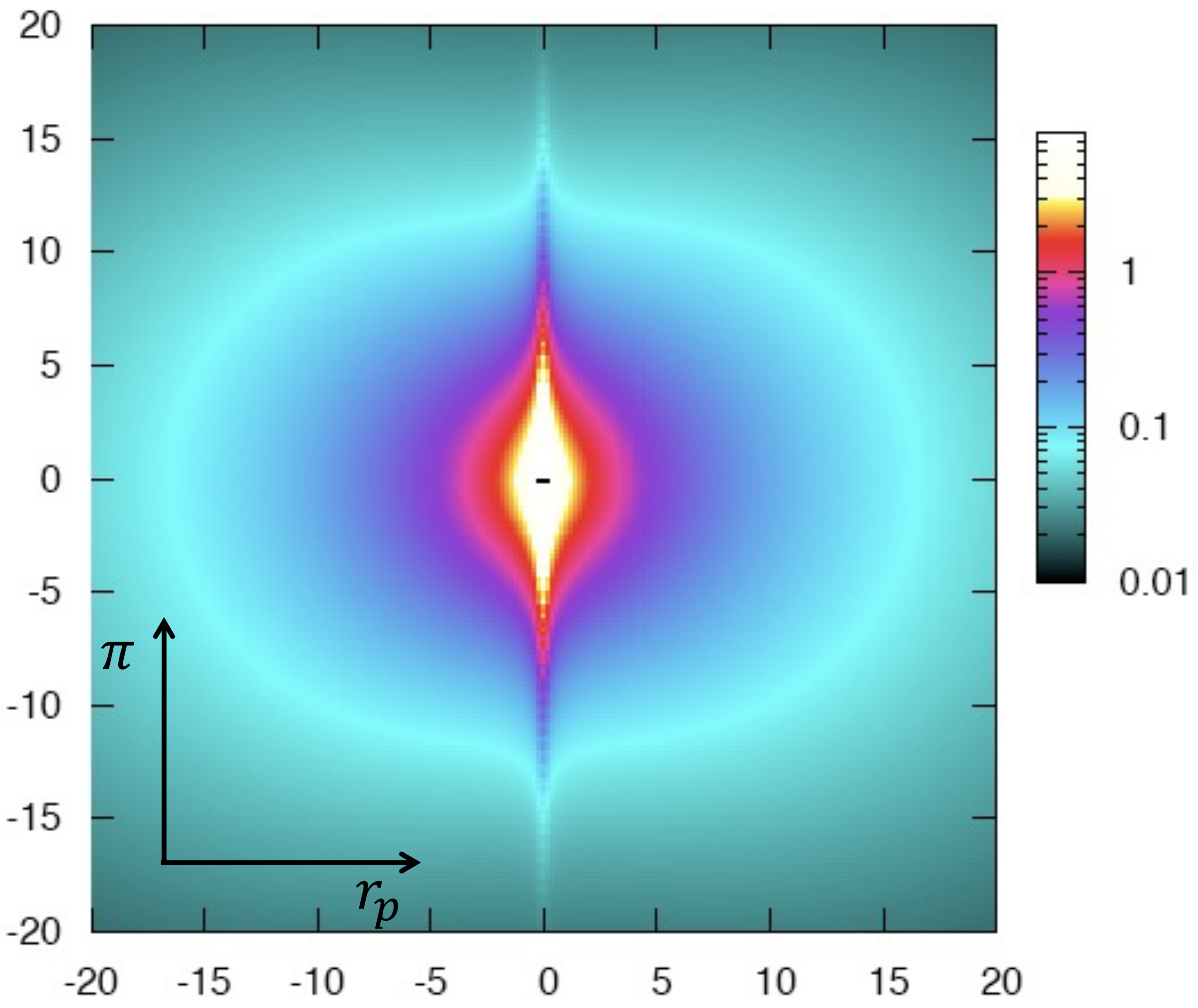

PECULIAR VELOCITIES

Let us justify the linear RSD term $\left[b\sigma_8(z) + f\sigma_8(z)\mu^2\right]^2$

$$n^s(\mathbf{s})\, d^3s = n(\mathbf{r})\, d^3r$$

Peculiar velocities conserve the galaxy number, $\boldsymbol{s}$ indicate the redshift-space coordinate r the real-space one. Their relation is $\boldsymbol{s} = \boldsymbol{r} + v\hat{\boldsymbol{r}}$ n is the galaxy number density.

after introducing fluctuations and mean values $\bar{n}(\boldsymbol{s})[1+\delta^s(\boldsymbol{s})]\, s^2 ds = \bar{n}(\boldsymbol{r})[1+\delta(\boldsymbol{r})]\, r^2 dr$

using the Jacobian of the coordinate transformation $1+\delta^s(\boldsymbol{s}) = \dfrac{r^2\bar{n}(\boldsymbol{r})}{(r+v)^2\bar{n}(\boldsymbol{r}+v\hat{\boldsymbol{r}})}\left(1+\dfrac{\partial v}{\partial r}\right)^{-1}[1+\delta(\boldsymbol{r})]$

keeping only linear order terms: $\delta^s(\boldsymbol{r}) = \delta(\boldsymbol{r}) - \left(\dfrac{\partial}{\partial r} + \dfrac{\alpha(\boldsymbol{r})}{r}\right) v$ where $\alpha(\boldsymbol{r}) \equiv \dfrac{\partial \ln r^2\bar{n}(\boldsymbol{r})}{\partial \ln r}$

To linear order the continuity equation reads: $v = -\beta \dfrac{\partial}{\partial r}\nabla^{-2}\delta$.

The linear redshift distortion operator $\boldsymbol{S}$; $\delta^s = \boldsymbol{S}\delta$ is then $\boxed{\mathbf{S} = 1 + \beta\left(\dfrac{\partial^2}{\partial r^2} + \dfrac{\alpha(\boldsymbol{r})\partial}{r\partial r}\right)\nabla^{-2}}$

PECULIAR VELOCITIES

$$\boxed{\mathbf{S} = 1 + \beta\left(\frac{\partial^2}{\partial r^2} + \frac{\alpha(\boldsymbol{r})\partial}{r\partial r}\right)\nabla^{-2}}$$

In the plane-parallel, distant observer limit: $\mathbf{S}^p = 1 + \beta\frac{\partial^2}{\partial z^2}\nabla^{-2}$ where $\beta = f/b$ and we assumed linear bas

In Fourier space the linear RS operator can be written as $\mathbf{S}^p = 1 + \beta\mu_{\boldsymbol{k}}^2$

Therefore, the relation between the Fourier coefficients in redshift and real space is $\hat{\delta}^s(\boldsymbol{k}) = (1 + \beta\mu_{\boldsymbol{k}}^2)\hat{\delta}(\boldsymbol{k})$

And the relation between the galaxy power spectra is $P^s(\boldsymbol{k}) = (1 + \beta\mu_{\boldsymbol{k}}^2)^2 P(\boldsymbol{k})$

Recalling that we are considering galaxy power spectra and that, having assumed linear bias $P(k) = b^2 P_m(k)$

$$\boxed{P_{obs}(k,\mu) = (b\sigma_8 + f\sigma_8\mu^2)^2\frac{P_m(k)}{\sigma_8^2}}$$

Non-linear Peculiar velocities

$$P_{\rm obs}(k_{\rm ref},\mu_{\rm ref};z) = \frac{1}{q_\perp^2 q_\parallel}\left\{\frac{\left[b\sigma_8(z)+f\sigma_8(z)\mu^2\right]^2}{1+\left[f(z)k\mu\sigma_{\rm p}(z)\right]^2}\right\}\frac{P_{\rm dw}(k,\mu;z)}{\sigma_8^2(z)}F_z(k,\mu;z)+P_{\rm s}(z)\,,$$

The distortion effect induced by nonlinear velocities, a.k.a. fingers of god effect, is modeled as a Lorenzian whose width is determined by the galaxy-galaxy velocity dispersion σ_p (which does not need to coincide with σ_v). It assumes that the 1-point velocity distribution function of the galaxies is well approximated by an exponential (Hamiltion 1998).

Alcock-Paczynski effect

$$P_{\rm obs}(k_{\rm ref},\mu_{\rm ref};z) = \frac{1}{q_\perp^2 q_\parallel}\left\{\frac{\left[b\sigma_8(z)+f\sigma_8(z)\mu^2\right]^2}{1+[f(z)k\mu\sigma_{\rm p}(z)]^2}\right\}\frac{P_{\rm dw}(k,\mu;z)}{\sigma_8^2(z)}F_z(k,\mu;z)+P_{\rm s}(z)$$

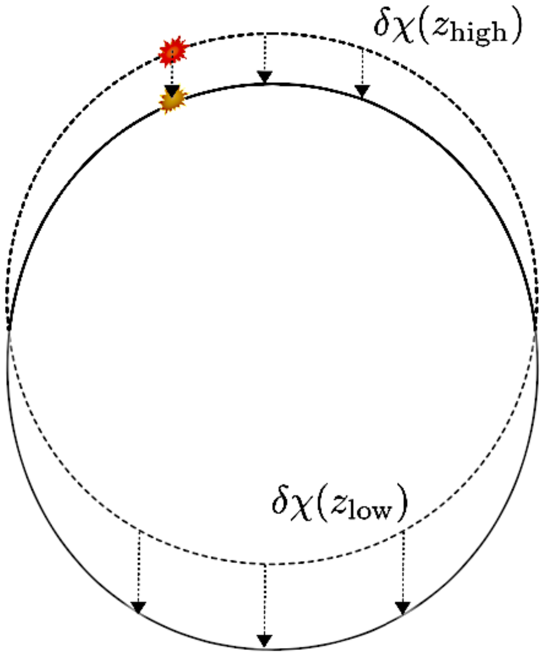

observer

To measure 2-point statistics we need to assume a fiducial cosmological model to transform redshifts into distances.

In general, the fiducial cosmology does not coincide with the true one. The bias introduced by using the incorrect cosmological model displaces, to first order, objects along the line of sight by some quantity $\delta\chi$ that, however, depends on the redshift. This creates a geometrical distortion called Alcock-Paczinsky effect. As a result, a spherical object will look a-spherical. For the same reason, the 2PCF iso-correlation contours will not be circles anymore.

Alcock-Paczynski effect

On the measured power spectrum the use of an incorrect cosmology leads to a rescaling of the component of the wavenumber vector $\boldsymbol{k}$ parallel and perpendicular to the line of sight, $k_{\parallel}$ $k_{\perp}$:

$$k_{\perp} = \frac{k_{\perp,\mathrm{ref}}}{q_{\perp}} \quad k_{\parallel} = \frac{k_{\parallel,\mathrm{ref}}}{q_{\parallel}}$$

, where the rescaling factors are $q_{\perp}(z) = \frac{D_{\mathrm{A}}(z)}{D_{\mathrm{A,\,ref}}(z)}$ and $q_{\parallel}(z) = \frac{H_{\mathrm{ref}}(z)}{H(z)}$

These scaling relations can be used to convert from the reference cosmology k_{ref}, μ_{ref} to the true one: μ, k:

$$k(k_{\mathrm{ref}}, \mu_{\mathrm{ref}}) = \frac{k_{\mathrm{ref}}}{q_{\perp}}\left[1 + \mu_{\mathrm{ref}}^2\left(\frac{q_{\perp}^2}{q_{\parallel}^2} - 1\right)\right]^{1/2} \quad \mu(\mu_{\mathrm{ref}}) = \mu_{\mathrm{ref}}\frac{q_{\perp}}{q_{\parallel}}\left[1 + \mu_{\mathrm{ref}}^2\left(\frac{q_{\perp}^2}{q_{\parallel}^2} - 1\right)\right]^{-1/2}$$

And these can be used to model the distortions on the observed power spectrum (Ballinger 1996)

$$\boxed{P_{\mathrm{proj,lin}}(k_{\mathrm{ref}}, \mu_{\mathrm{ref}};\ z) = \frac{1}{q_{\perp}^2 q_{\parallel}} P_{\mathrm{zs,lin}}(k(k_{\mathrm{ref}}, \mu_{\mathrm{ref}}), \mu(\mu_{\mathrm{ref}}); z)}$$

Shot Noise

Redshift errors

$$P_{\mathrm{obs}}(k_{\mathrm{ref}},\mu_{\mathrm{ref}};z)=\frac{1}{q_\perp^2 q_\parallel}\left\{\frac{\left[b\sigma_8(z)+f\sigma_8(z)\mu^2\right]^2}{1+[f(z)k\mu\sigma_{\mathrm{p}}(z)]^2}\right\}\frac{P_{\mathrm{dw}}(k,\mu;z)}{\sigma_8^2(z)}F_z(k,\mu;z)+P_{\mathrm{s}}(z)\,,$$

The shot noise error P_s due to Poisson sampling by target galaxies is equal to $\frac{n_k}{N}$ where N=number of galaxies and n_k= number of k-modes in the k-bin. The shot noise error is usually subtracted at the estimator level. If so, $P_s(z)$ accounts for possible residuals.

3D clustering analyses rely on spectroscopically measured redshifts. The statistical uncertainty in their measurement is $\sigma_z = O(100)Km\ s^{-1}$. Their effect is to smear the galaxy density field along the line of sight. These errors propagate into comoving distance errors $\sigma_r = c/H(z)\sigma_z$. and their effect can be modeled as $F_z(k,\mu;z)=\mathrm{e}^{-k^2\mu^2\sigma_r^2(z)}$

Photometric vs. spectroscopic redshift surveys

Photometric vs. spectroscopic Redshifts

Spectroscopic redshifts are estimated by measuring the wavelength of some characteristic feature identified in galaxy spectra. Their typical relative error is $\sigma_z/(1+z)\sim 10^{-3}$.

Photometric redshifts are faster to measure but $O(50)$ times less precise than the spectroscopic ones. The number of objects with measured photometric redshifts correspondingly increases.
Smearing along the line of sight is more severe. It erases the clustering signal on a scale of tens of Mpc. As a result a full 3D clustering analysis is useless. Tomographic techniques are used instead.

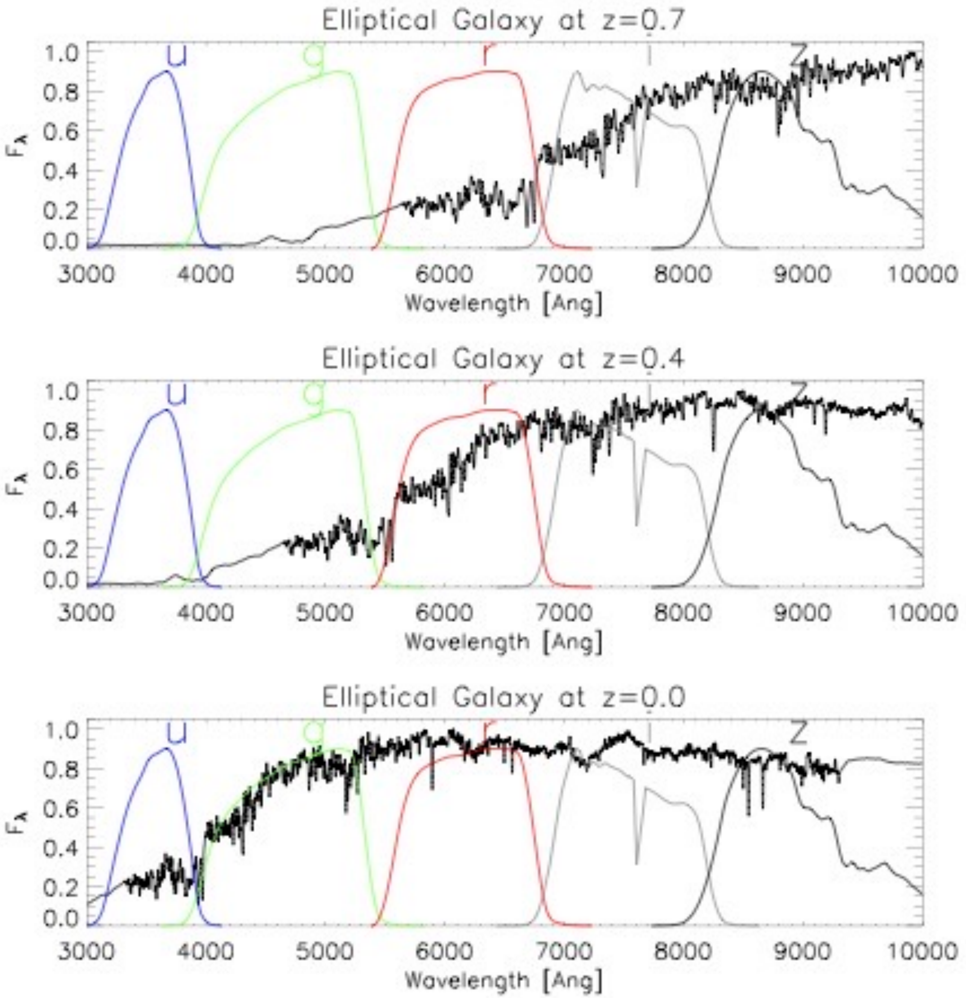

Padmanabhan+ 2007

Photometric Redshifts

In a photo-z survey, one can divide the catalog into subsamples of objects placed in different redshift bins *i,j...* and characterized by their redshift distribution $n_i(z)$.

The auto- or cross-angular correlations (or spectra) can be estimated by correlating the projected overdensity of objects at different angular separations. The corresponding double integral can be simplified using the Limber approximation valid at small separations, providing.

$$\boxed{C_{ij}^{XY}(\ell) = \frac{c}{H_0}\int_{z_{\rm min}}^{z_{\rm max}} \mathrm{d}z\, \frac{W_i^X(k_\ell, z) W_j^Y(k_\ell, z)}{E(z) r^2(z)} P_{\delta\delta}^{XY}(k_\ell, z)}$$

Where X,Y identify the tracer (galaxies in this case). $H_0 E(z) = H(z)$. r=comoving distance. $P_{\delta\delta}^{GG}$ = matter power spectrum evaluated at $k_\ell = \left(\ell + \frac{1}{2}\right)/r(z)$. ij identify the two z-bins

$$\boxed{W_i^{\rm G}(k, z) = \frac{H_0}{c} b_i(k, z) \frac{n_i(z)}{\bar{n}_i} E(z)}$$

with $b(k,z)$ scale- and redshift-dependent bias.

Photometric Redshifts

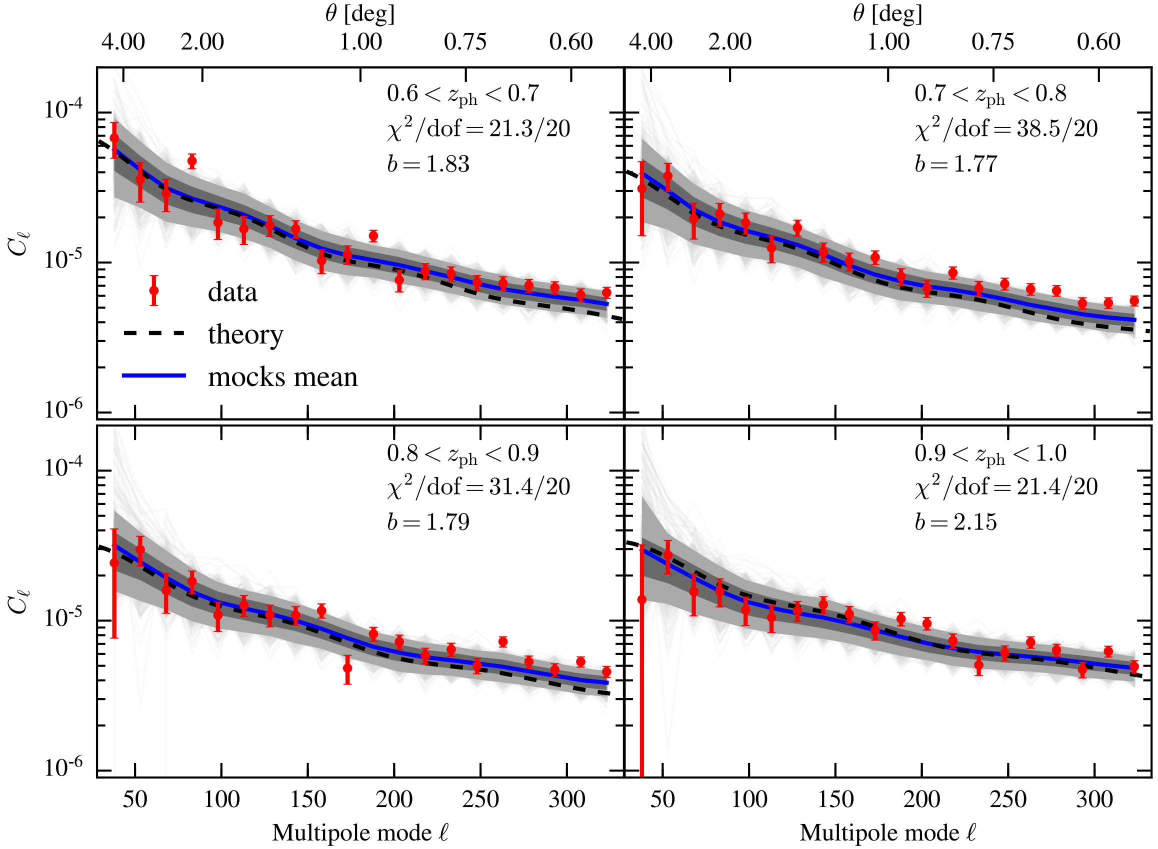

Camacho+ 2018 DES Y1

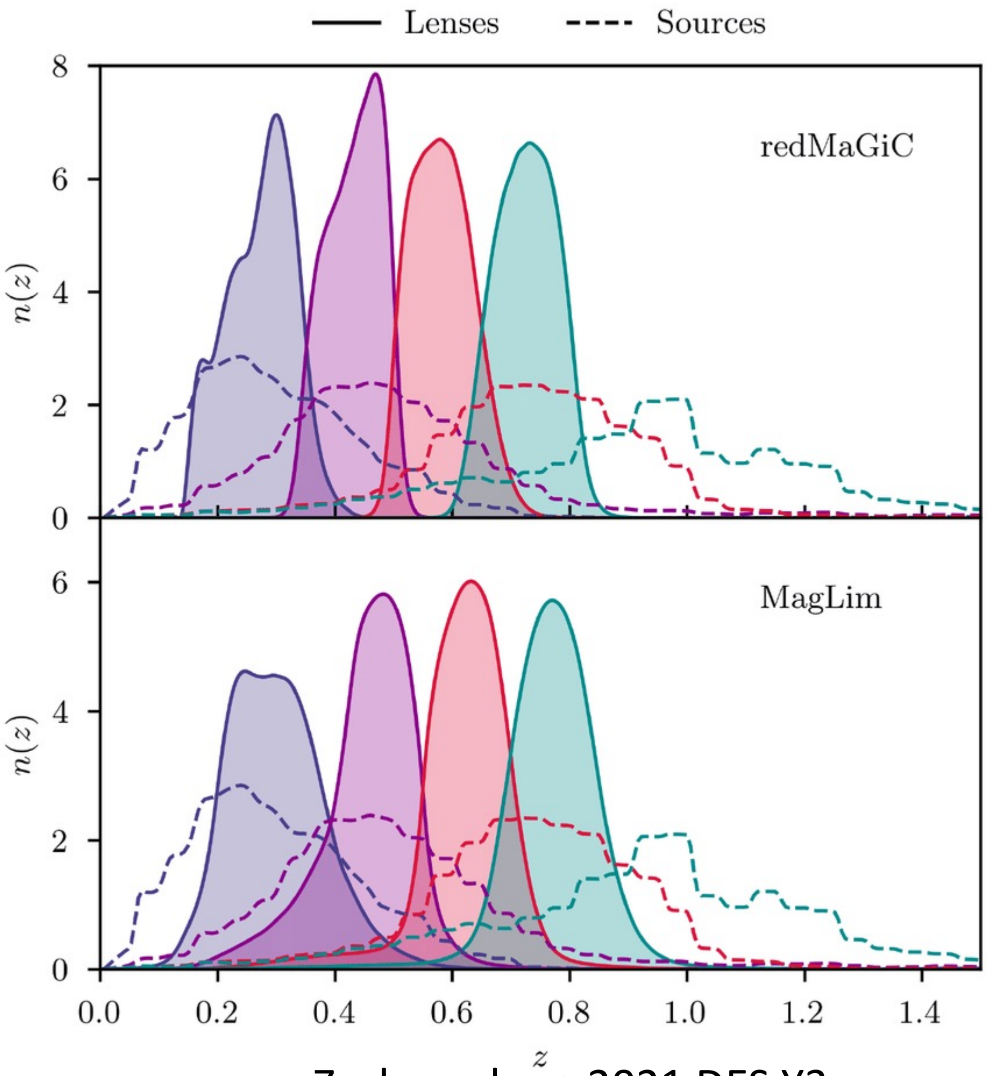

Zacharegkas+ 2021 DES Y3

Beyond clustering statistics: lensing

Gravitational Lensing

The same tomographic analysis can be performed for the gravitational lensing effect, rather than galaxies.

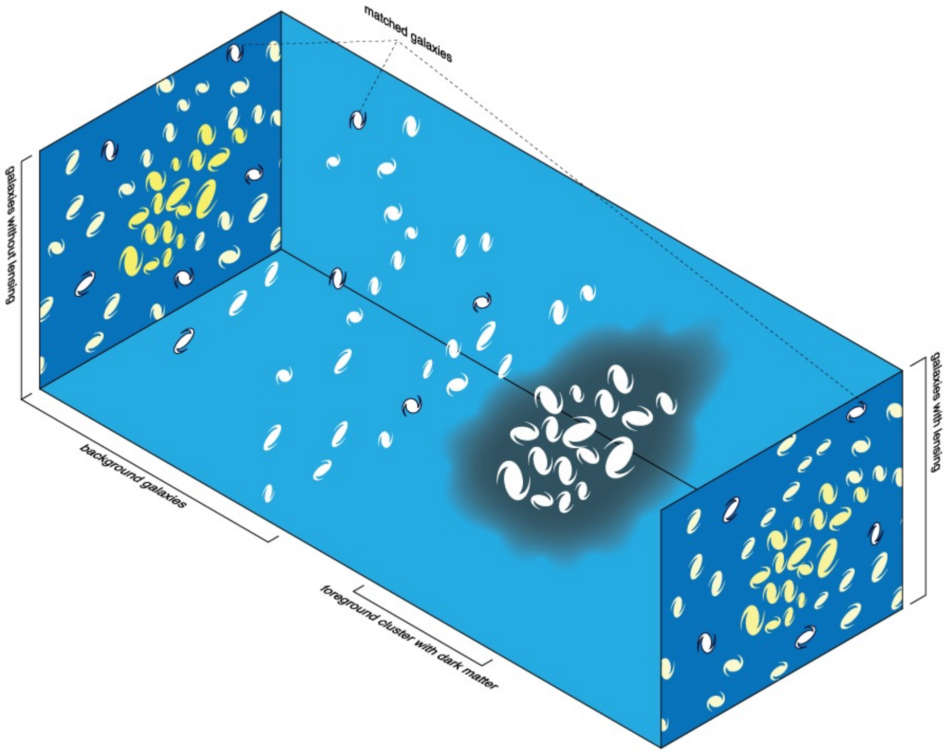

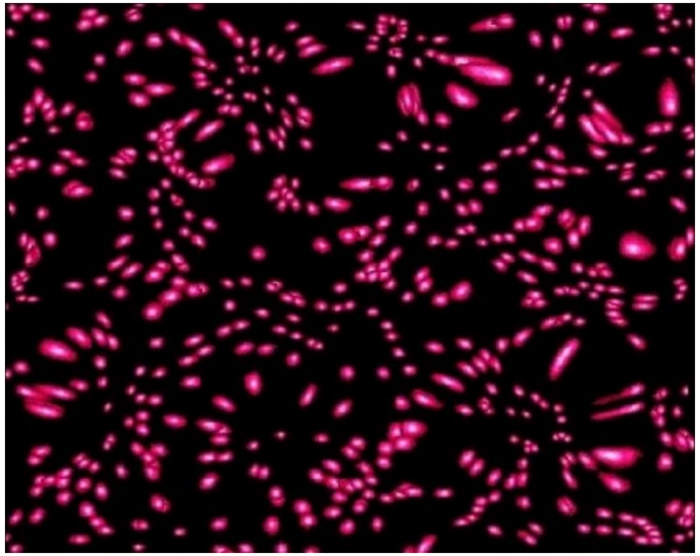

Image credit: Smoot lensing subgroup

This can be done by measuring the systematic ellipticity distortions of distant "lensed" galaxies by the intervening matter distribution.
The procedure of the tomographic analysis is the same as for galaxies except for the window function, which is different, and for the data, which is not galaxy positions but lensing shear maps.

Gravitational Lensing

$$C_{ij}^{XY}(\ell) = \frac{c}{H_0}\int_{z_{\rm min}}^{z_{\rm max}} \mathrm{d}z\, \frac{W_i^X(k_\ell,z)W_j^Y(k_\ell,z)}{E(z)r^2(z)} P_{\delta\delta}^{XY}(k_\ell,z)$$

with $X{=}Y{=}L$ this expression identifies the auto-spectrum of the lensing signal. In this case

$$W_i^{\rm L}(k,z) = \frac{3}{2}\Omega_{{\rm m},0}\frac{H_0^2}{c^2}(1+z)r(z)\int_z^{z_{\rm max}} \mathrm{d}z' \frac{n_i(z)}{\bar{n}_i}\frac{r(z'-z)}{r(z')} \quad + W_i^{\rm IA}(k,z)$$

W_i^{IA} quantifies the contribution of the galaxy intrinsic alignment, modeled as:

$$W_i^{\rm IA}(k,z) = -\frac{\mathcal{A}_{\rm IA}\mathcal{C}_{\rm IA}\Omega_{{\rm m},0}\mathcal{F}_{\rm IA}(z)}{D(z,k)}\frac{n_i(z)}{\bar{n}_i(z)}\frac{H_0}{c}E(z)$$

where $\mathcal{F}_{IA}$ depends on the galaxy luminosity function and $\mathcal{A},\mathcal{C}$ ... are parameters

- The lensing-lensing spectrum does not depend on galaxy bias.
- Tomographic analyses also include galaxy-lensing spectra.
- For galaxy clustering analyses (including tomographic GG) $P_{\delta\delta} = P_{cc}$. For lensing analyses $P_{\delta\delta} = P_{mm}$. For GL $P_{\delta\delta} = \sqrt{P_{cc} + P_{mm}}$

Lensing & Clustering

Clustering and lensing probe different regions of the k-space.
Because of the radial smearing, tomographic analyses probe a limited interval of small $k_{\parallel}$ values but thanks to high angular resolution are sensitive to large $k_{\perp}$ (large ℓ) values.
As a result, a fully nonlinear model for the power spectrum is used in the tomographic analyses whereas for clustering analyses the use of SPT or EFT models is usually sufficient.

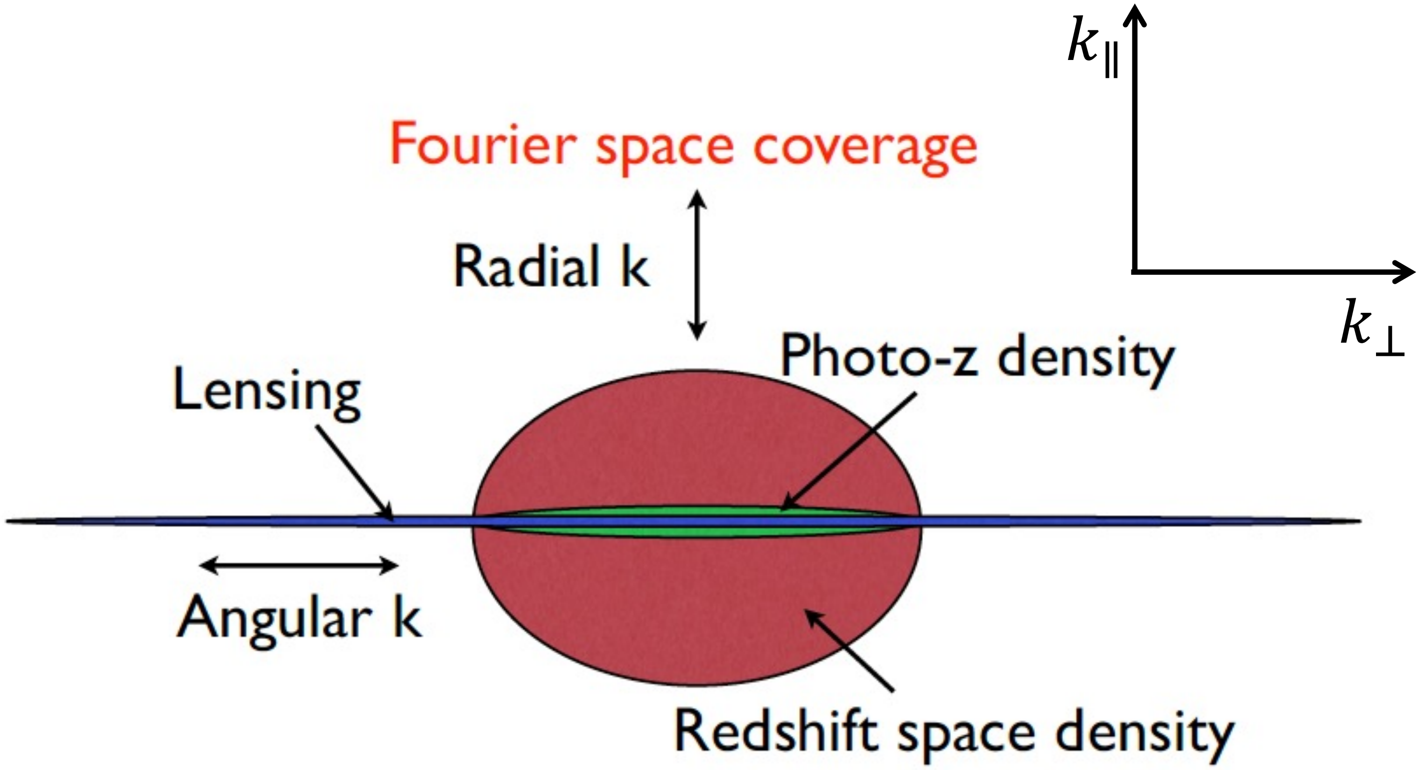

Datasets

ONGOING AND FUTURE SURVEYS

Photometric Surveys

Spectroscopic Surveys

- Rubin
- DES
- Euclid
- Roman
- SKA
- J-PAS
- DESI
- Prime Focus Spectrograph
- HETDEX
- 4MOST
- Sphere^{X}

Optimizing surveys: DESI

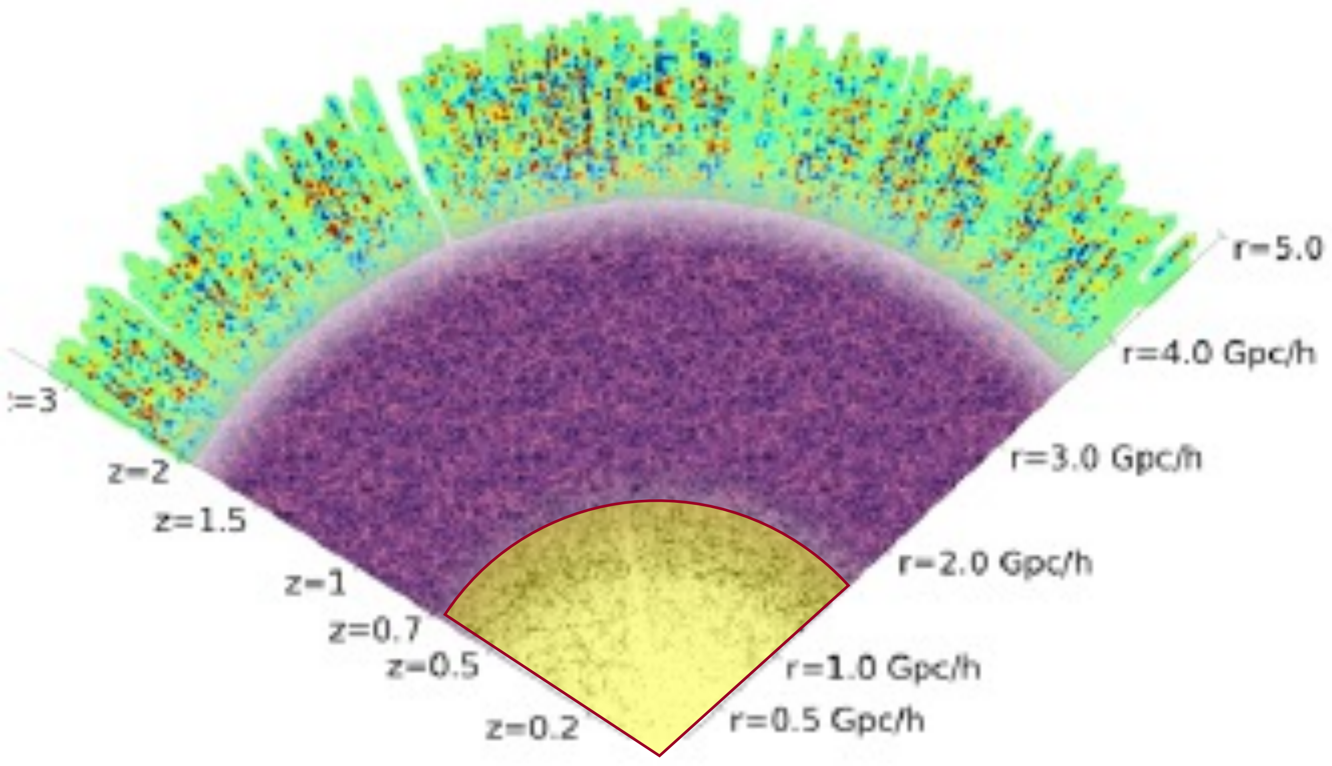

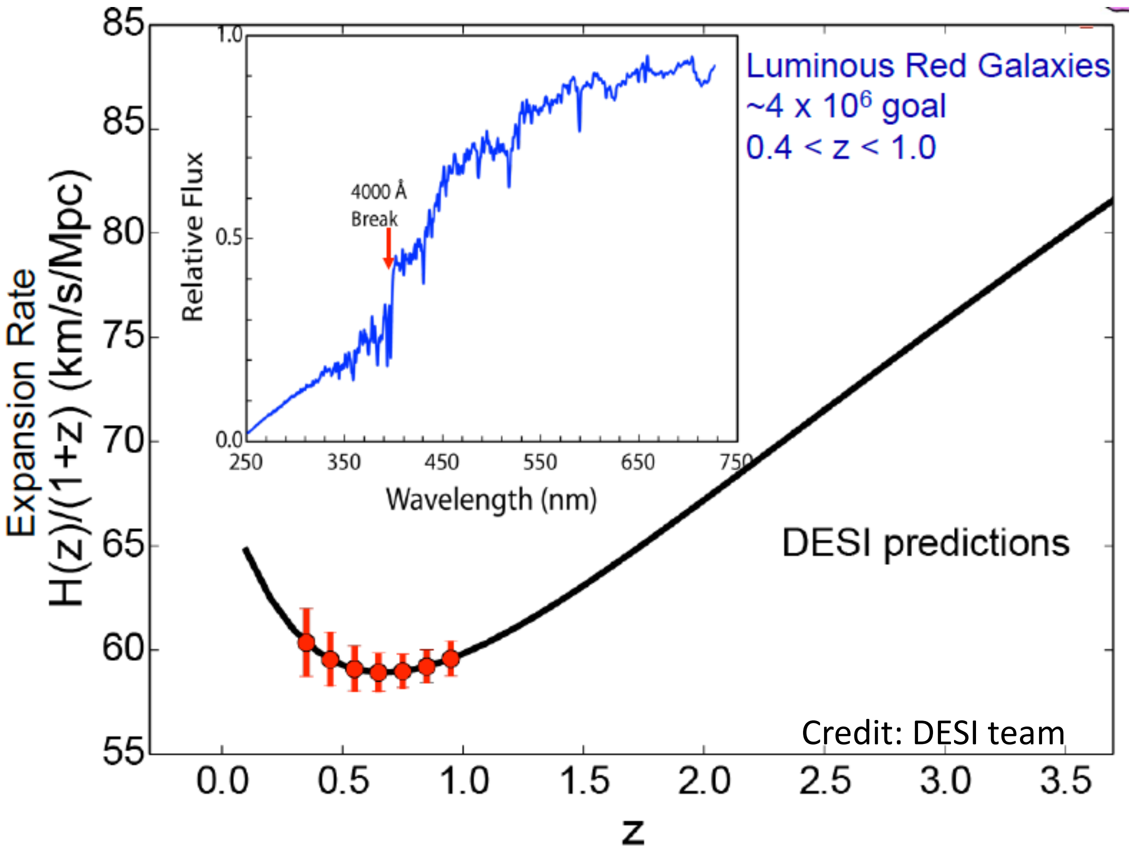

Optimizing surveys: DESI

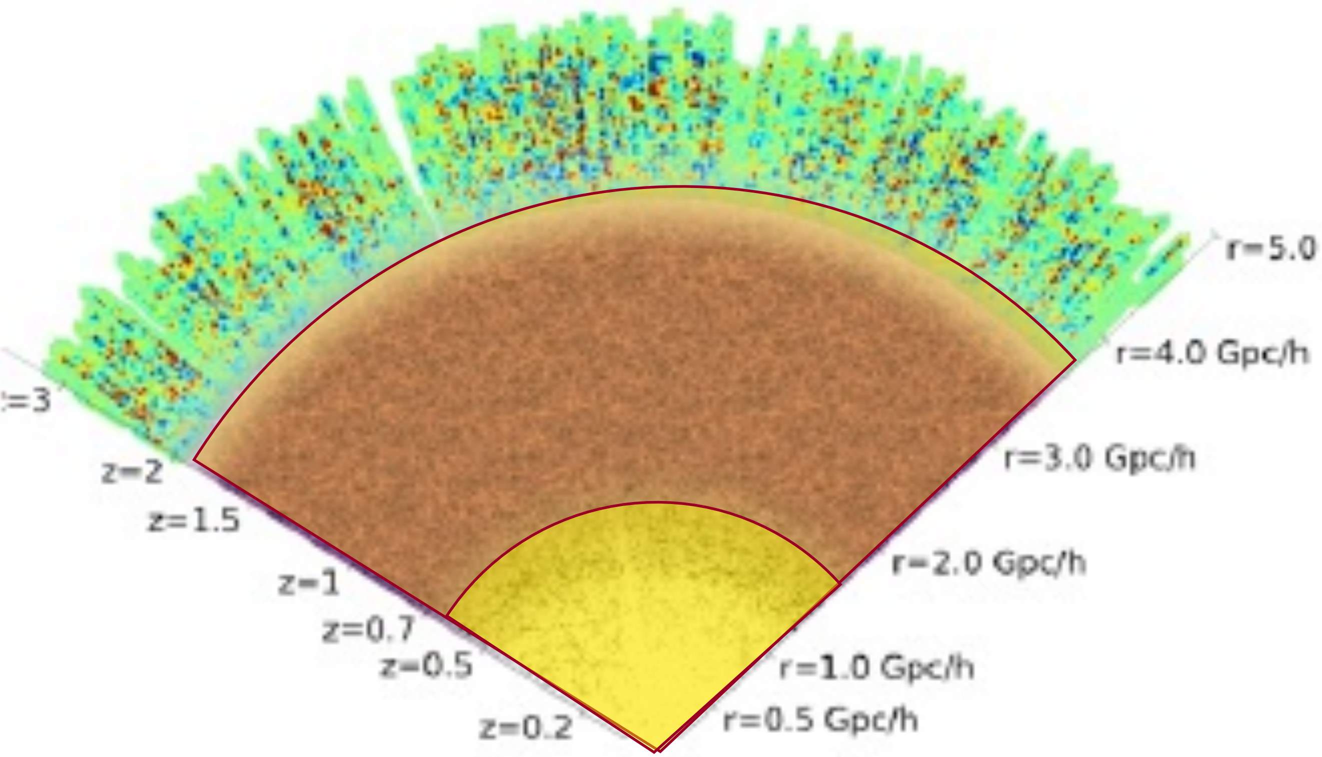

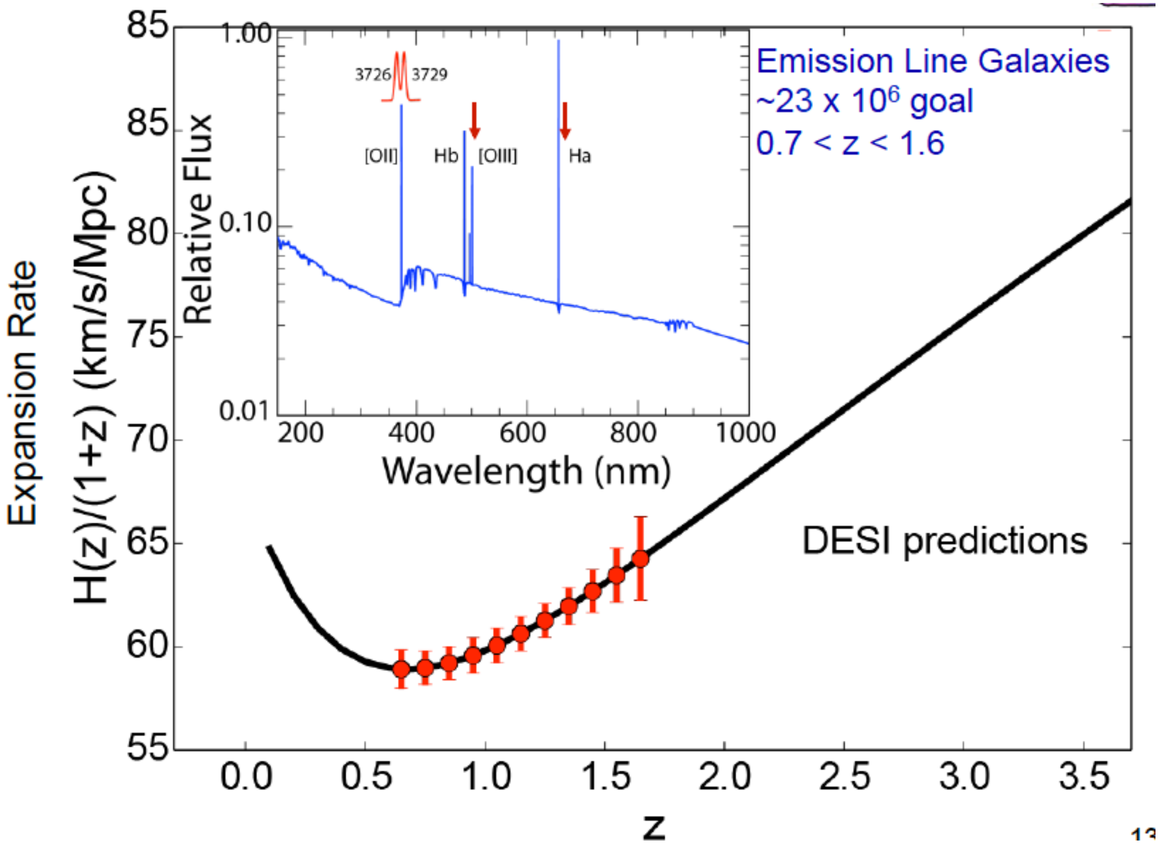

Optimizing surveys: DESI

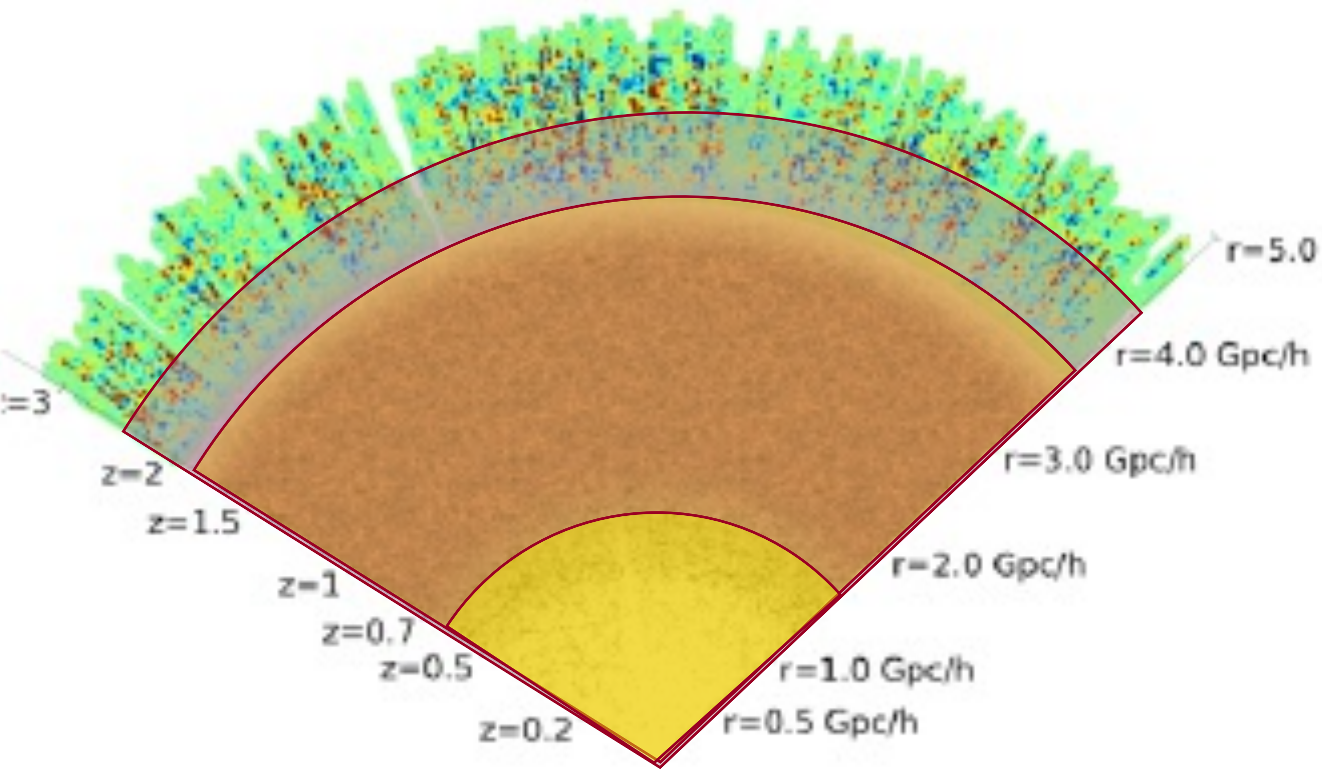

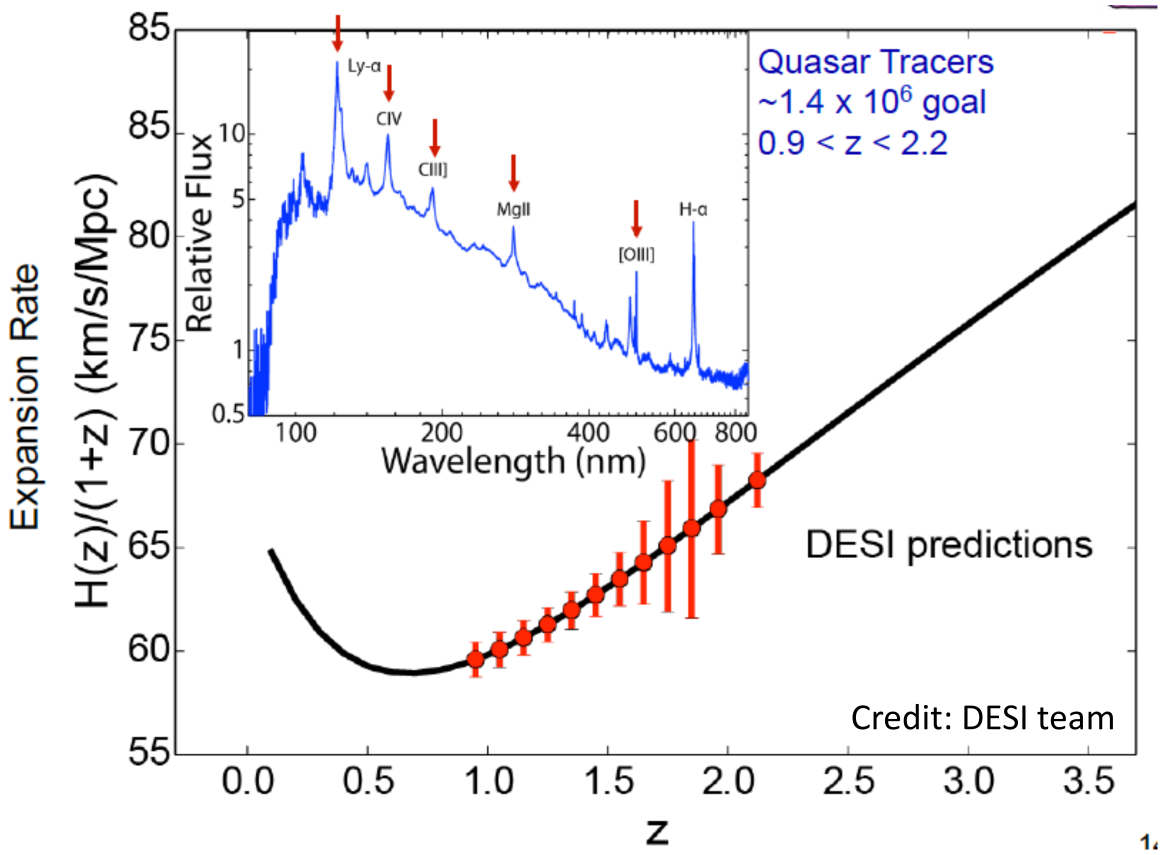

Credit: DESI team

Optimizing surveys: DESI

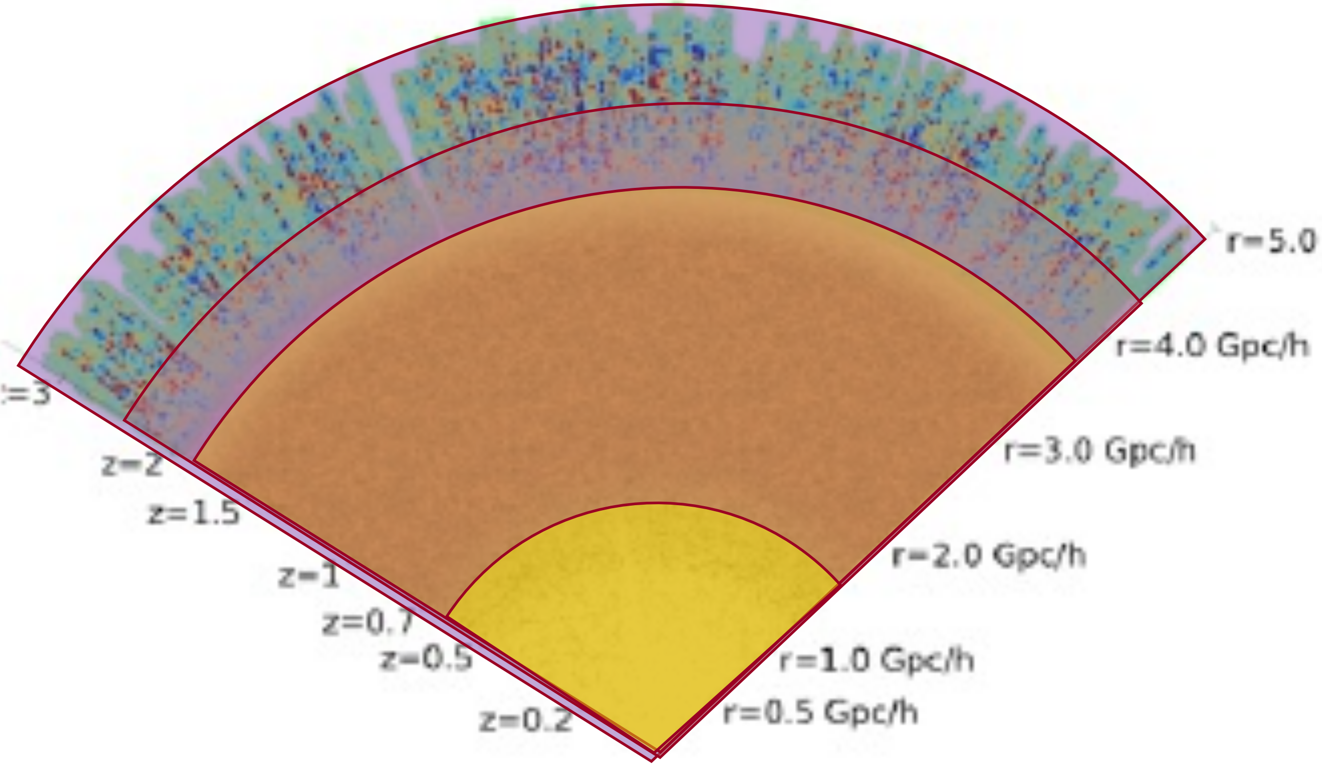

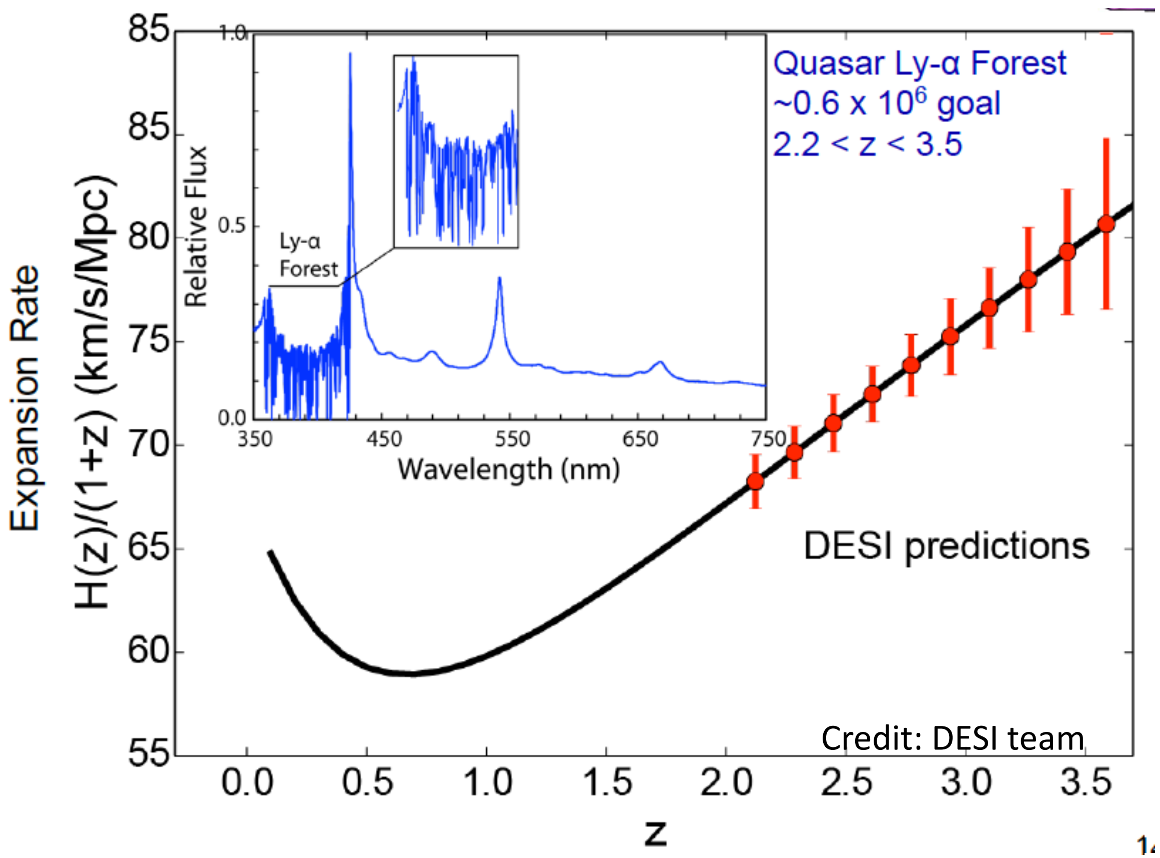

Optimizing surveys: DESI

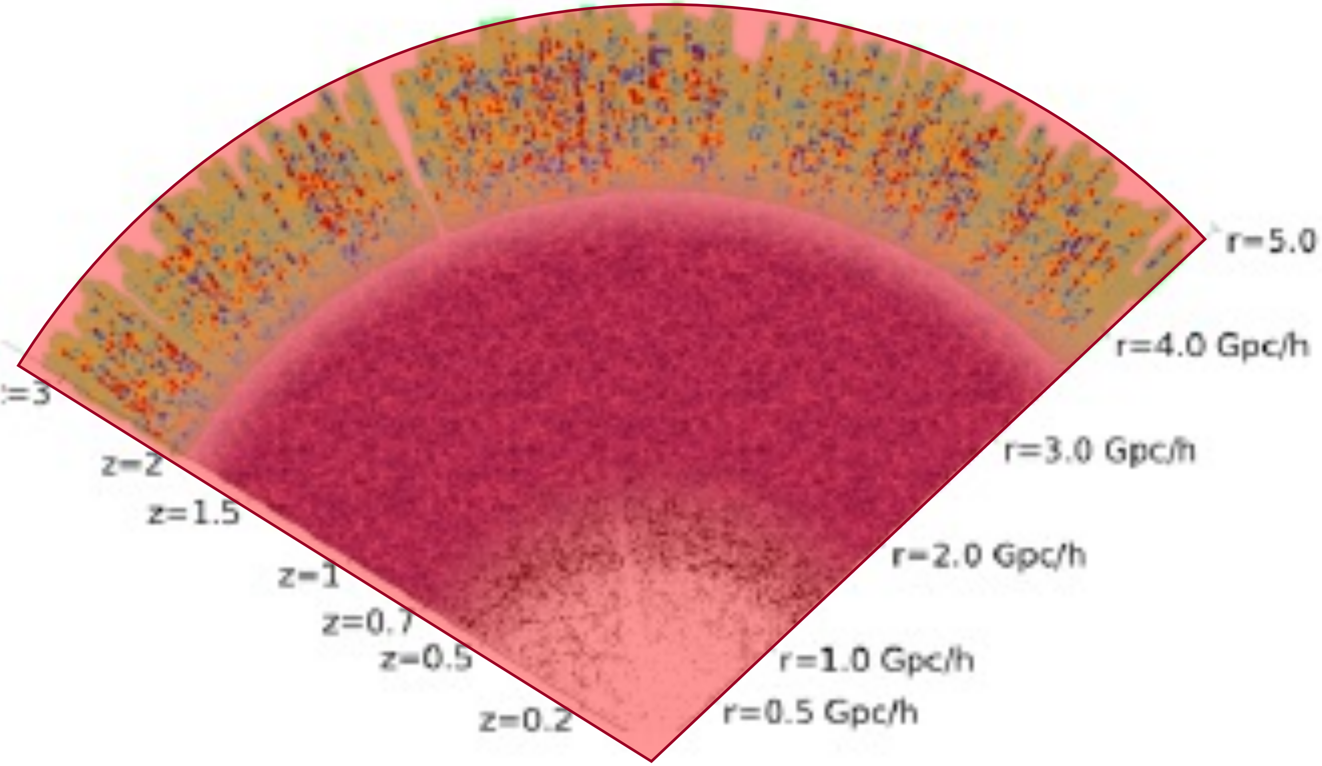

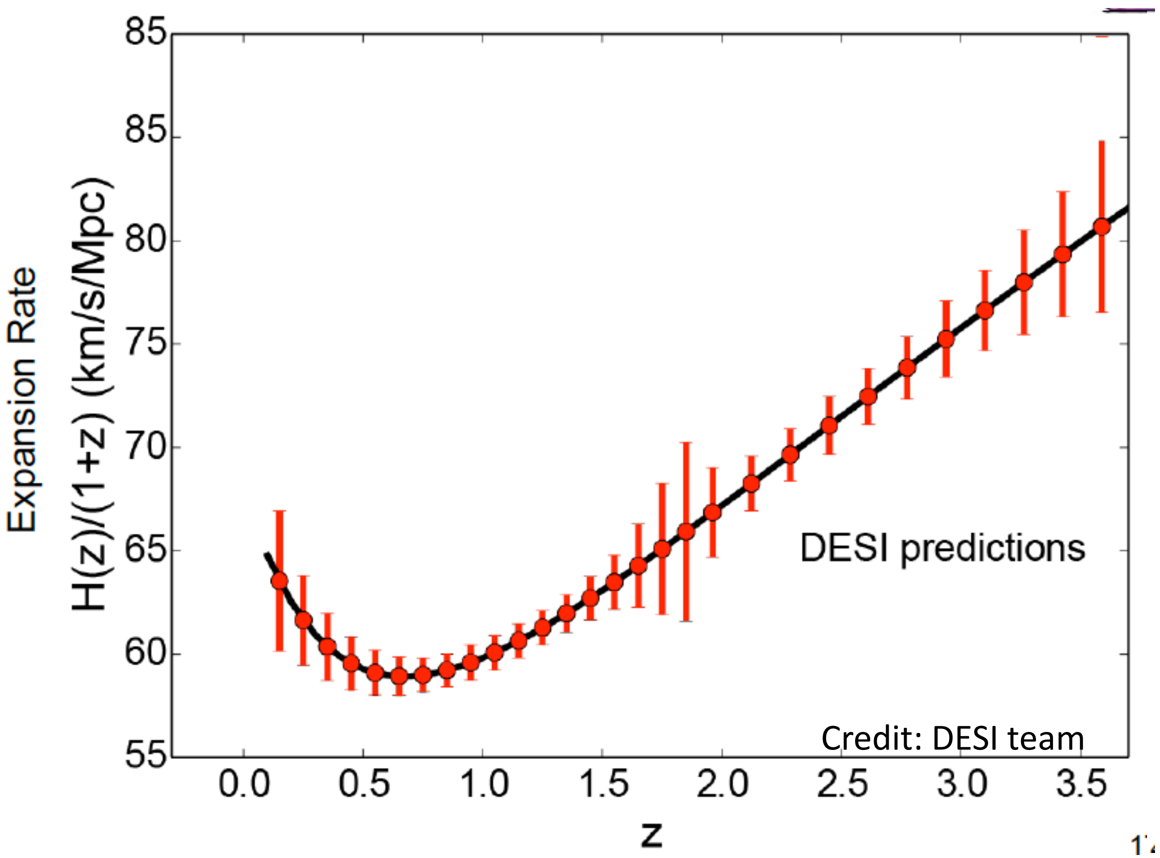

Surveys' complexity: Euclid

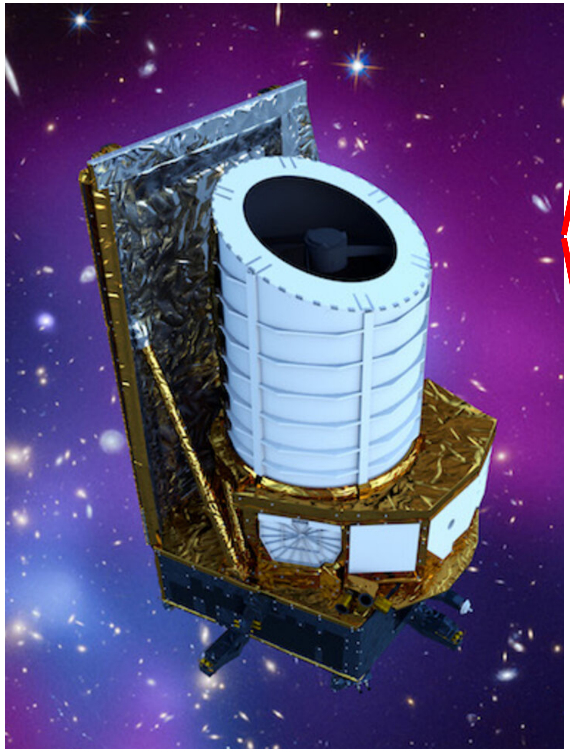

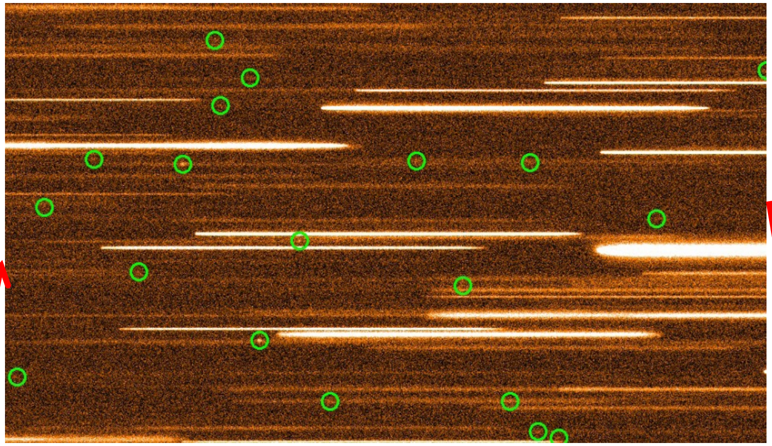

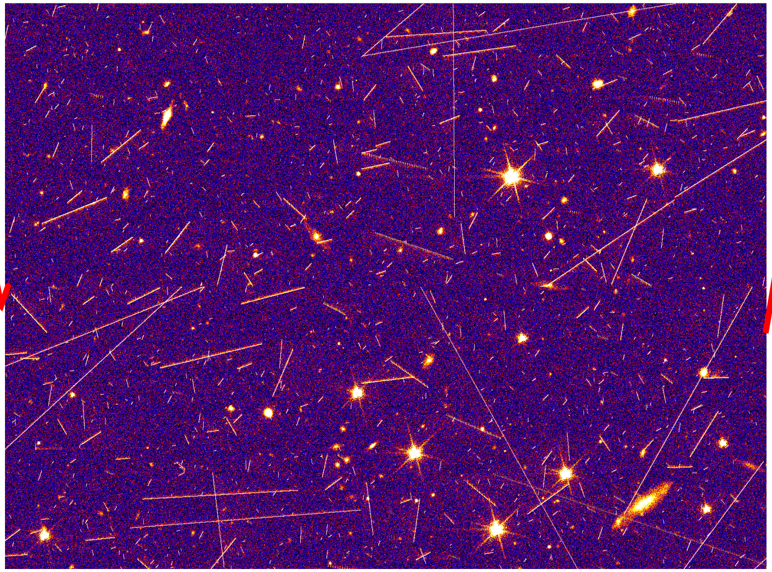

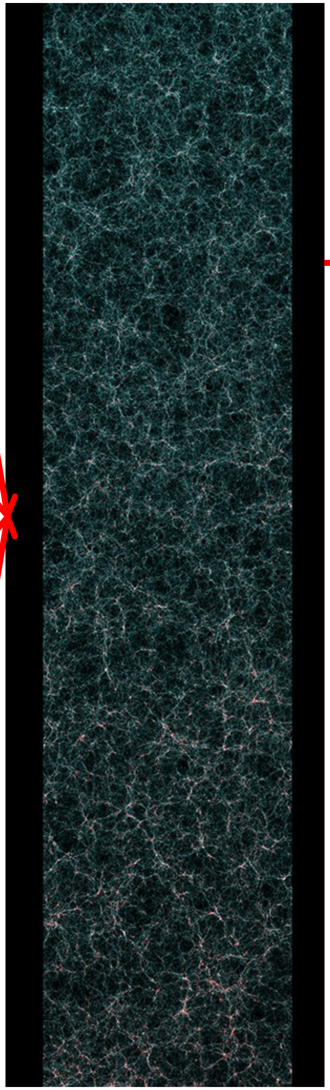

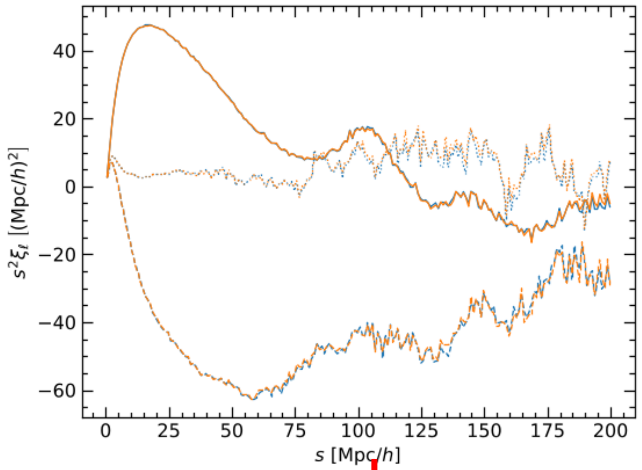

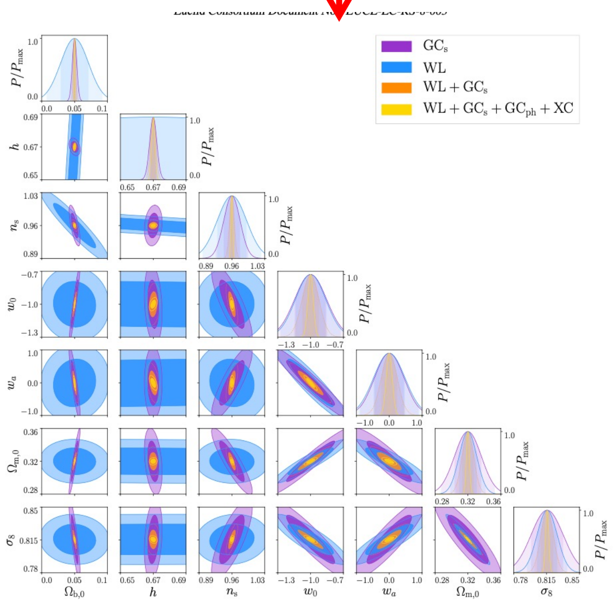

Large Scale Structures and Neutrinos

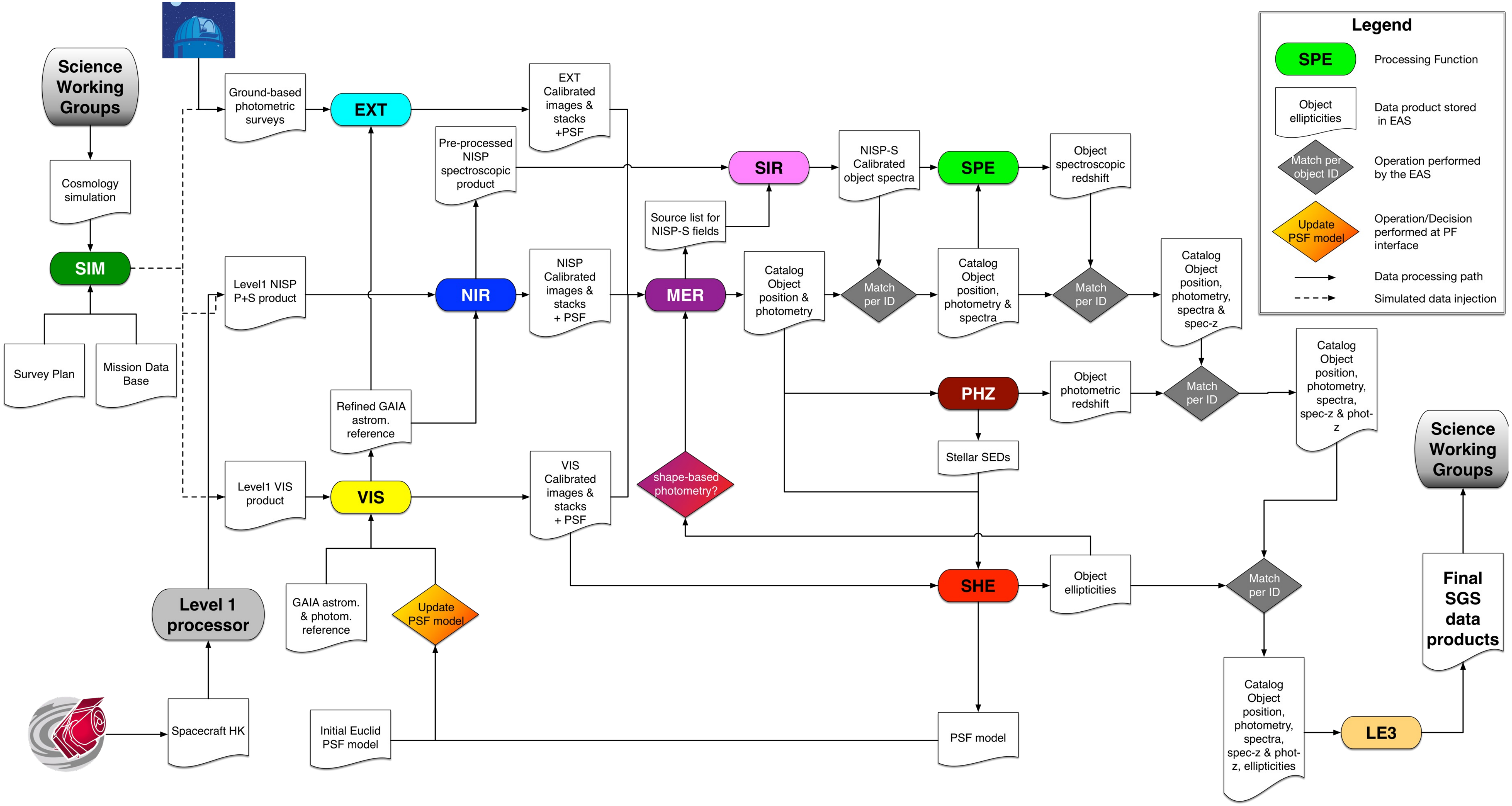

Redundancy Importance: an example

To guarantee % accuracy (matching the required precision) a large degree of redundancy is necessary, at the data level (independent datasets and reductions procedures) at the statistical analysis level (independent estimators), and at the parameter estimation level (independent models, independent data vs. model comparisons).

One example, relevant to clustering statistics, is the use of both the 3D power spectrum and the 2PCF: they are a Fourier pair with the same information content. And yet we use both. Why ?

The galaxy power spectrum and the impact of massive neutrinos on it is easier to model, especially during the linear regime, when the Fourier coefficients evolve separately. Efficient estimators have been proposed to account for selection effects that reduce the statistical completeness of the sample (i.e. the FKP estimator, Feldmann+ (1993)) and to reduce the wide-angle bias that affects the large-scale modes (Scoccimarro+ 2015, Bianchi+2015). Problems arise when dealing with a complex survey geometry.

REDUNDANCY IMPORTANCE: AN EXAMPLE

As an example of a realistic survey footprint let us consider that of the Euclid mission.

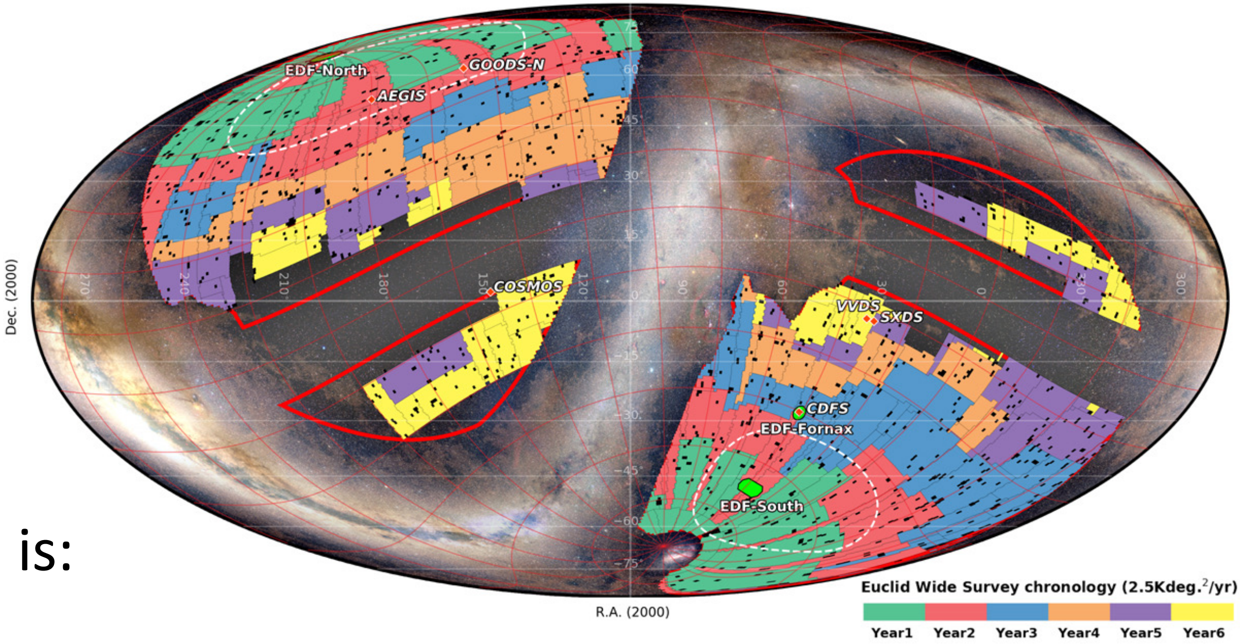

The angular footprint and the radial weight function $w(\boldsymbol{r})$ that quantifies selection effects define a survey window whose Fourier transform is:

$$G(\boldsymbol{k}) \propto \int d^3\boldsymbol{r}\, w(\boldsymbol{r})\, \bar{n}(\boldsymbol{r}) e^{i\boldsymbol{k}\cdot\boldsymbol{r}}$$

As a result, the measured power spectrum is a convolution of the true power spectrum with the window function $G(\boldsymbol{k})$:

$$\widehat{\boldsymbol{P}}(\boldsymbol{k}) \propto \int d^3\boldsymbol{q}\, P_{true}(\boldsymbol{k}-\boldsymbol{q})|G(\boldsymbol{q})|^2$$

whose accurate evaluation is challenging.

Redundancy Importance: an example

The 2-point correlation function is more challenging to model and less efficient to estimate.
However, 2PCF estimators are generally robust to selection effects and survey volume effects since in their case the excess probability associated with the 2-point function is estimated by comparing the pair counts of real galaxies *(DD)* with those of a sample of mock, unclustered "random" objects *(RR)* distributed over the same volume and suffering the same selection effects as the real survey.

$$\widehat{\xi}_{\rm N} = \frac{DD}{RR} - 1, \quad \widehat{\xi}_{\rm DP} = \frac{DD}{DR} - 1, \quad \widehat{\xi}_{\rm He} = \frac{DD - DR}{RR}, \quad \widehat{\xi}_{\rm Ha} = \frac{DD\ RR}{DR^2} - 1, \quad \widehat{\xi}_{\rm LS} = \frac{DD - 2DR + RR}{RR}.$$

The challenge (also for the estimate of the power spectrum) is to include all potential systematic effects in the random catalog with a sub-% accuracy to measure cosmological parameters AND the neutrino masses with the desired precision.

Neutrino mass

Constraints

Large Scale Structures and Neutrinos

Let us go back to the effect of neutrino masses on the matter power spectrum.

The dashed line shows the linear damping that we have already discussed (see insert) what we obtain when we include massive neutrino without changing the total mass density ω_m. In this case, massive neutrino is reduce the amplitude of the power spectrum on small scales. In the linear regime, the asymptotic reduction is proportional to f_ν.

However, keeping ω_m and ω_b constant (to satisfy cosmological nucleosynthesis and CMB constraints) while increasing the neutrino mass fraction would delay equivalence.

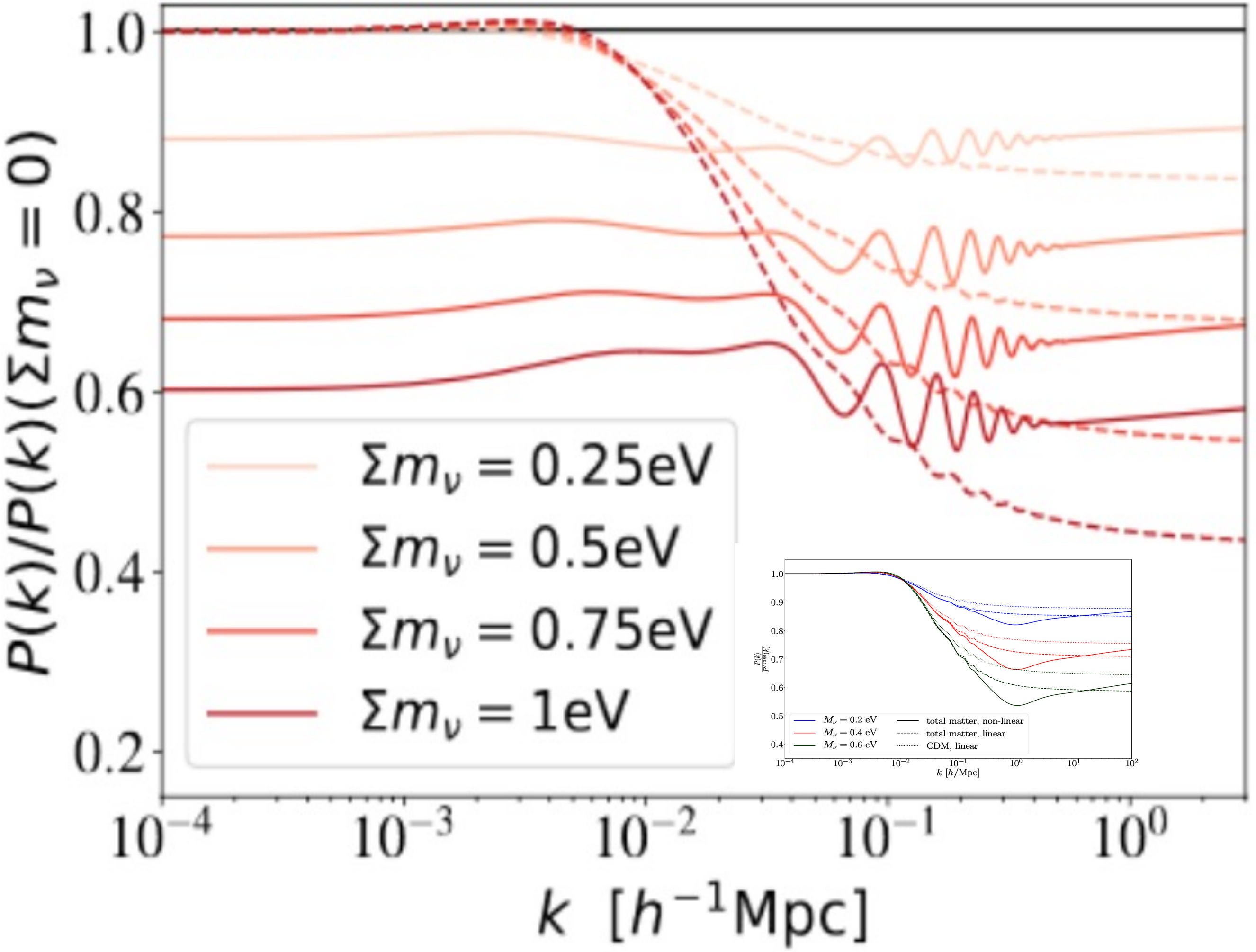

Lesgourues & Verde 2021

Let us go back to the effect of neutrino masses on the matter power spectrum.

The dashed line shows the linear damping that we have already discussed (see insert) what we obtain when we include massive neutrino without changing the total mass density ω_m. In this case, massive neutrino is reduce the amplitude of the power spectrum on small scales. In the linear regime, the asymptotic reduction is proportional to f_ν.

However, keeping ω_m and ω_b constant (to satisfy cosmological nucleosynthesis and CMB constraints) while increasing the neutrino mass fraction would delay equivalence.

$$a_{eq} = \frac{\omega_r}{\omega_{CDM} + \omega_b} = \frac{\omega_r}{\omega_m}(1 - f_\nu)^{-1}$$

Changing the equivalence epoch has a large effect on the CMB spectrum. Which is measured with high precision.

One wants, instead, to evaluate the impact of neutrino mass when keeping a_{eq} and ω_b constant in a flat ΛCDM universe.

The latter constraint reads: $\sum \Omega_i = 1$ i.e.

$$\frac{\omega_m}{h^2} + \Omega_\gamma + \Omega_\Lambda = 1$$

Large Scale Structures and Neutrinos

$$a_{eq} = \frac{\omega_r}{\omega_m}(1 - f_\nu)^{-1} \qquad \frac{\omega_m}{h^2} + \Omega_\gamma + \Omega_\Lambda = 1$$

An increase of ω_m from the first equation can be compensated by either a decrease of Ω_Λ or by and increase of h.
The first option would change the angular diameter distance to the last scattering surface and displace the BAO peaks.
A change in h would be less detectable in the CMB spectrum (ISW effect) but would decrease the overall amplitude of the power spectrum on large scales (continuous curves).
This degeneracy can be broken by the galaxy power spectrum (and its BAO peaks).

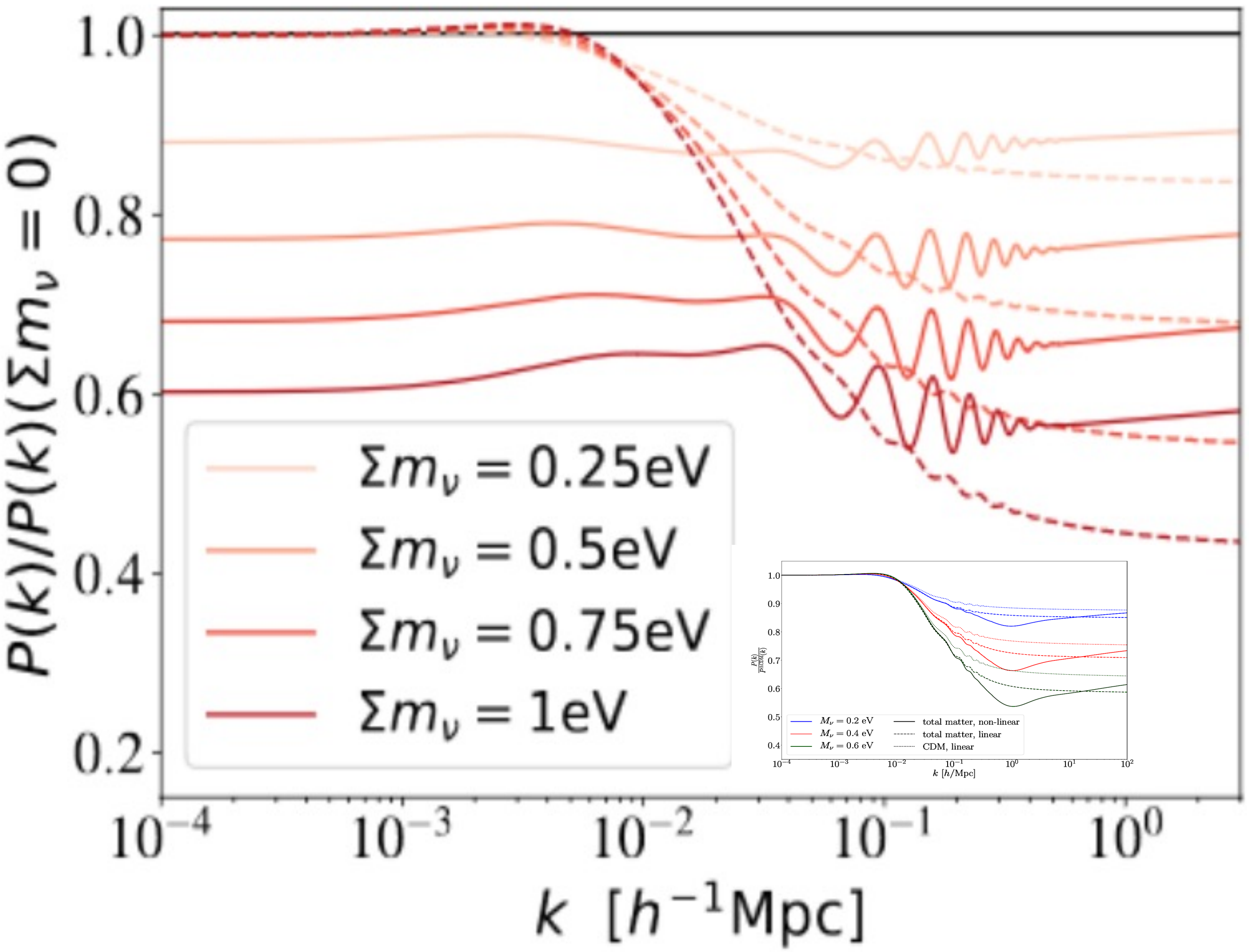

Lesgourues & Verde 2021

M_ν constraints from LSS

- Constraints from LSS alone are not very stringent.
- They are when combined with the CMB.
- Constraints from LSS are not very sensitive to N_{eff} (which is determined from the CMB).

M_ν CONSTRAINTS FROM LSS

Table from Lesgourgues & Verde 2021

	Model	95% CL (eV)
CMB alone		
Pl18[TT+lowE]	ΛCDM+$\sum m_\nu$	< 0.54
Pl18[TT,TE,EE+lowE]	ΛCDM+$\sum m_\nu$	< 0.26
CMB + probes of background evolution		
Pl18[TT+lowE] + BAO	ΛCDM+$\sum m_\nu$	< 0.13
Pl18[TT,TE,EE+lowE]+BAO	ΛCDM+$\sum m_\nu$+5 params.	< 0.515
CMB + LSS		
Pl18[TT+lowE+lensing]	ΛCDM+$\sum m_\nu$	< 0.44
Pl18[TT,TE,EE+lowE+lensing]	ΛCDM+$\sum m_\nu$	< 0.24
CMB + probes of background evolution + LSS		
Pl18[TT,TE,EE+lowE] + BAO + RSD	ΛCDM+$\sum m_\nu$	< 0.10
Pl18[TT+lowE+lensing] + BAO + Lyman-α	ΛCDM+$\sum m_\nu$	< 0.087
Pl18[TT,TE,EE+lowE] + BAO + RSD + Pantheon + DES	ΛCDM+$\sum m_\nu$	< 0.13

Planck 2018

M_ν constraints from LSS

BAO breaks
h-degeneracy

Table from Lesgourgues & Verde 2021

	Model	95% CL (eV)
CMB alone		
Pl18[TT+lowE]	ΛCDM+$\sum m_\nu$	< 0.54
Pl18[TT,TE,EE+lowE]	ΛCDM+$\sum m_\nu$	< 0.26
CMB + probes of background evolution		
Pl18[TT+lowE] + BAO	ΛCDM+$\sum m_\nu$	< 0.13
Pl18[TT,TE,EE+lowE]+BAO	ΛCDM+$\sum m_\nu$+5 params.	< 0.515
CMB + LSS		
Pl18[TT+lowE+lensing]	ΛCDM+$\sum m_\nu$	< 0.44
Pl18[TT,TE,EE+lowE+lensing]	ΛCDM+$\sum m_\nu$	< 0.24
CMB + probes of background evolution + LSS		
Pl18[TT,TE,EE+lowE] + BAO + RSD	ΛCDM+$\sum m_\nu$	< 0.10
Pl18[TT+lowE+lensing] + BAO + Lyman-α	ΛCDM+$\sum m_\nu$	< 0.087
Pl18[TT,TE,EE+lowE] + BAO + RSD + Pantheon + DES	ΛCDM+$\sum m_\nu$	< 0.13

Planck 2018

+ EBOSS. Alam+ 2021

M_ν Constraints from LSS

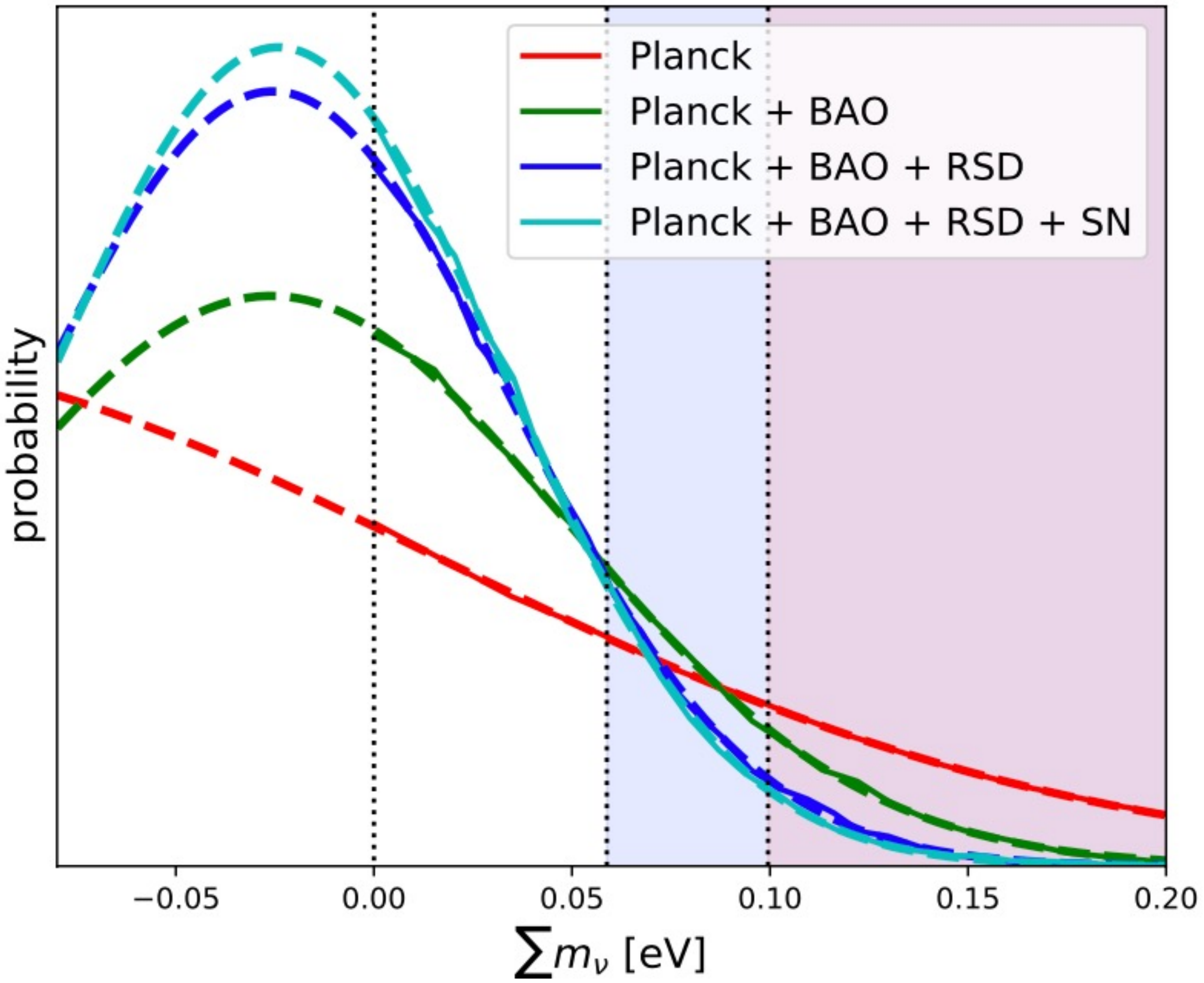

BAO breaks
h-degeneracy

EBOSS. Alam+ 2021

M_ν Constraints from LSS

RSD adds info and breaks bias degeneracy.

Table from Lesgourgues & Verde 2021

	Model	95% CL (eV)
CMB alone		
Pl18[TT+lowE]	ΛCDM+$\sum m_\nu$	< 0.54
Pl18[TT,TE,EE+lowE]	ΛCDM+$\sum m_\nu$	< 0.26
CMB + probes of background evolution		
Pl18[TT+lowE] + BAO	ΛCDM+$\sum m_\nu$	< 0.13
Pl18[TT,TE,EE+lowE]+BAO	ΛCDM+$\sum m_\nu$+5 params.	< 0.515
CMB + LSS		
Pl18[TT+lowE+lensing]	ΛCDM+$\sum m_\nu$	< 0.44
Pl18[TT,TE,EE+lowE+lensing]	ΛCDM+$\sum m_\nu$	< 0.24
CMB + probes of background evolution + LSS		
Pl18[TT,TE,EE+lowE] + BAO + RSD	ΛCDM+$\sum m_\nu$	< 0.10
Pl18[TT+lowE+lensing] + BAO + Lyman-α	ΛCDM+$\sum m_\nu$	< 0.087
Pl18[TT,TE,EE+lowE] + BAO + RSD + Pantheon + DES	ΛCDM+$\sum m_\nu$	< 0.13

Planck 2018

+ EBOSS. Alam+ 2021

+ EBOSS. Alam+ 2021

M_ν Constraints from LSS

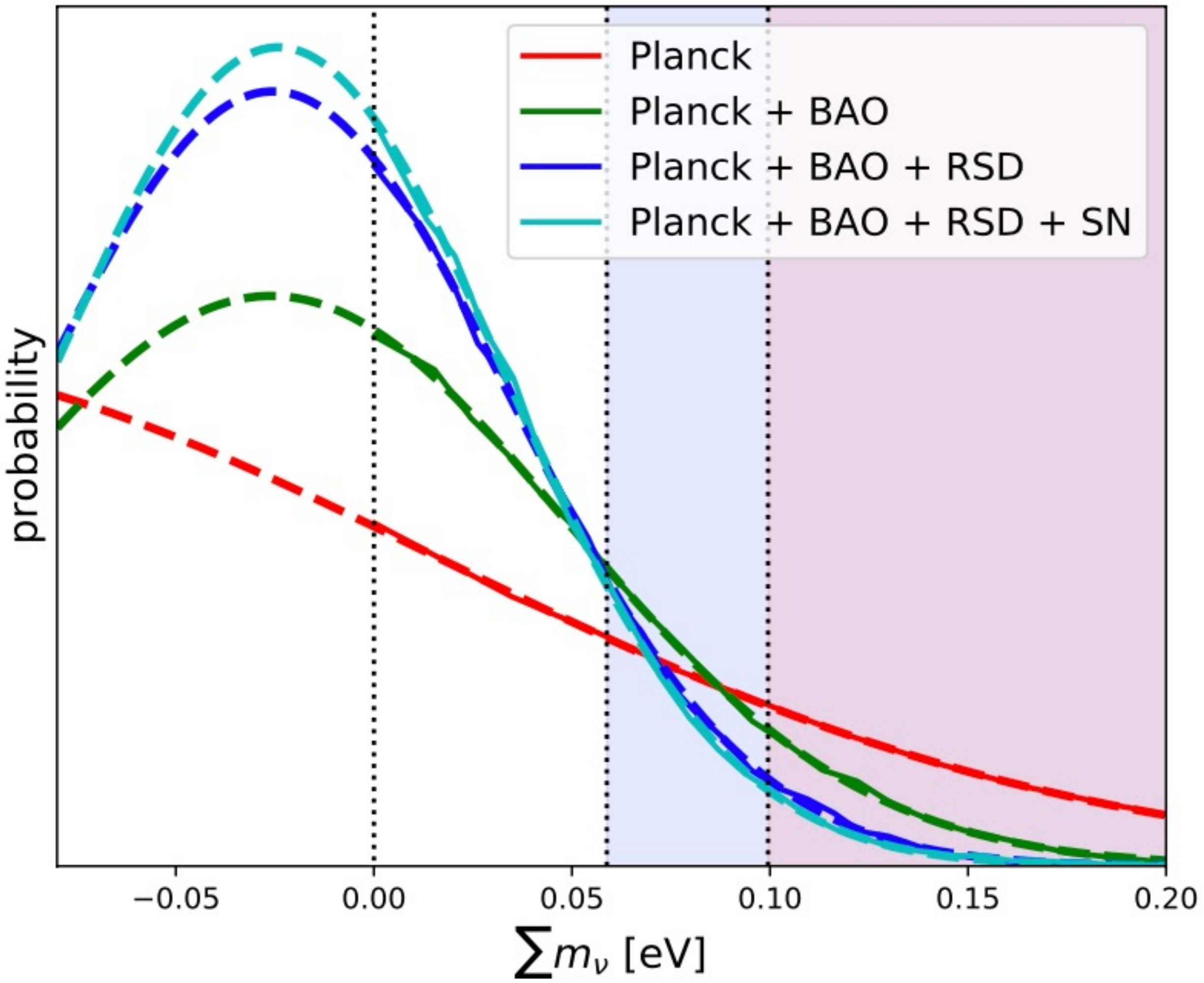

BAO breaks h-degeneracy

EBOSS. Alam+ 2021

M_ν CONSTRAINTS FROM LSS

Low-z lenses → low clustering amplitude S_8 → higher M_ν

Table from Lesgourgues & Verde 2021

	Model	95% CL (eV)	
CMB alone			
Pl18[TT+lowE]	ΛCDM+$\sum m_\nu$	< 0.54	
Pl18[TT,TE,EE+lowE]	ΛCDM+$\sum m_\nu$	< 0.26	Planck 2018
CMB + probes of background evolution			
Pl18[TT+lowE] + BAO	ΛCDM+$\sum m_\nu$	< 0.13	+ EBOSS. Alam+ 2021
Pl18[TT,TE,EE+lowE]+BAO	ΛCDM+$\sum m_\nu$+5 params.	< 0.515	
CMB + LSS			
Pl18[TT+lowE+lensing]	ΛCDM+$\sum m_\nu$	< 0.44	
Pl18[TT,TE,EE+lowE+lensing]	ΛCDM+$\sum m_\nu$	< 0.24	
CMB + probes of background evolution + LSS			
Pl18[TT,TE,EE+lowE] + BAO + RSD	ΛCDM+$\sum m_\nu$	< 0.10	+ EBOSS. Alam+ 2021
Pl18[TT+lowE+lensing] + BAO + Lyman-α	ΛCDM+$\sum m_\nu$	< 0.087	
Pl18[TT,TE,EE+lowE] + BAO + RSD + Pantheon + DES	ΛCDM+$\sum m_\nu$	< 0.13	+ DES Y3 Abbott+ 2021

M_ν CONSTRAINTS FROM LSS

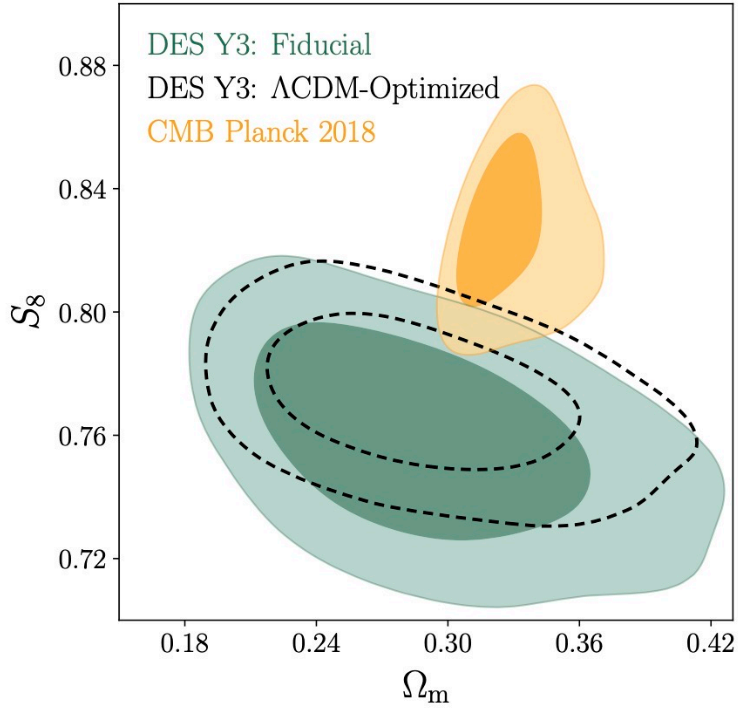

DES Y3 Amon+ 2023

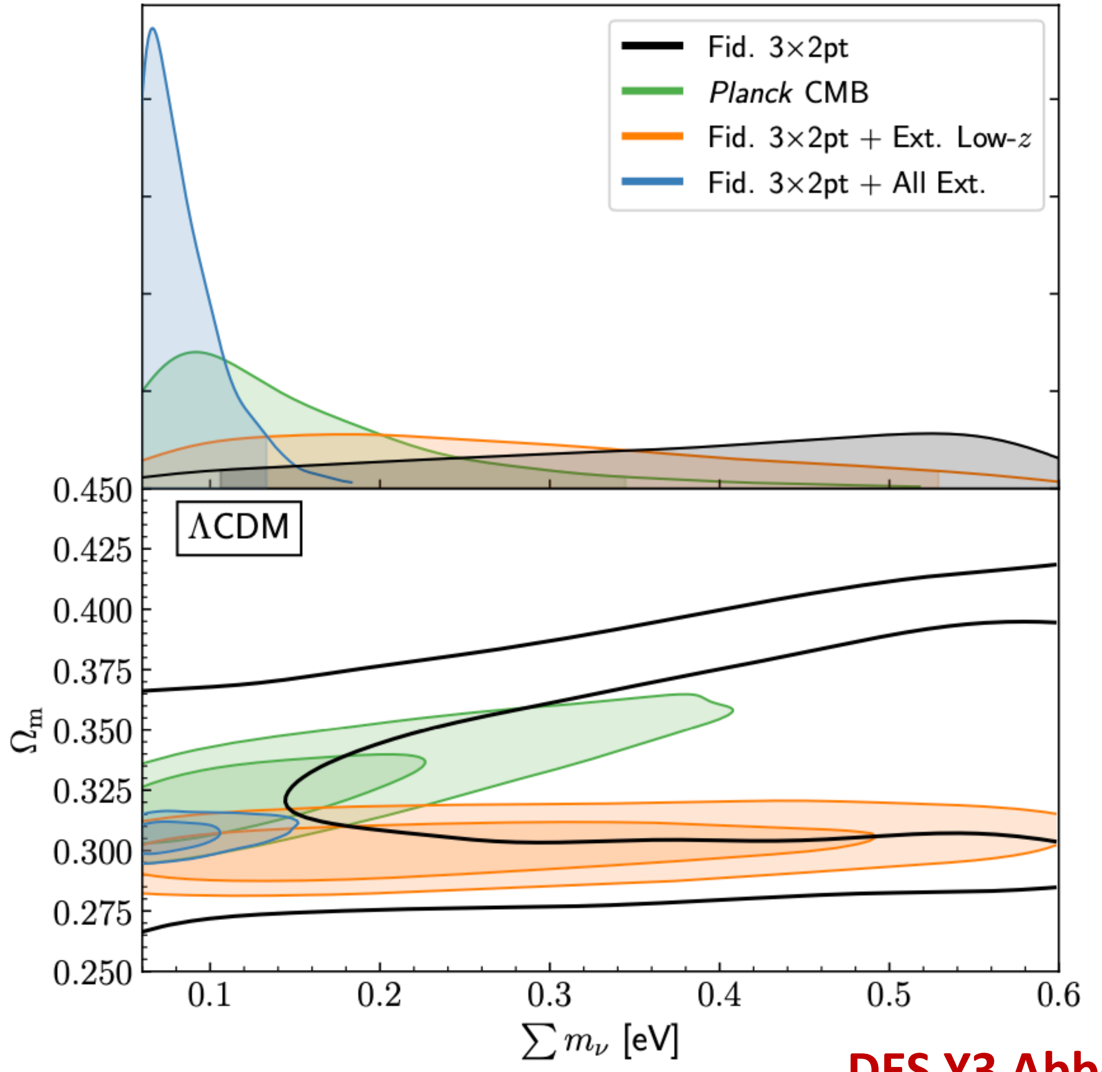

DES Y3 Abbott+ 2021

Low-z lenses → low clustering amplitude S_8 → higher M_ν

$$S_8 = \sigma_8\sqrt{\Omega_M/0.3}$$

BAO vs. Full Shape

	$\nu\Lambda$CDM		
Parameter	Planck	Planck + BAO	Planck + FS
$100\ \omega_b$	$2.238^{+0.016}_{-0.015}$	$2.245^{+0.014}_{-0.014}$	$2.247^{+0.015}_{-0.013}$
ω_{cdm}	$0.1201^{+0.0013}_{-0.0014}$	$0.11919^{+0.00099}_{-0.00099}$	$0.11893^{+0.00097}_{-0.001}$
$100\ \theta_s$	$1.04187^{+0.00030}_{-0.00030}$	$1.04195^{+0.00029}_{-0.00029}$	$1.04196^{+0.00028}_{-0.00028}$
τ	$0.0543^{+0.0074}_{-0.0079}$	$0.05556^{+0.007}_{-0.0076}$	$0.05539^{+0.0074}_{-0.0072}$
$\ln(10^{10} A_s)$	$3.045^{+0.014}_{-0.016}$	$3.045^{+0.014}_{-0.015}$	$3.044^{+0.014}_{-0.014}$
n_s	$0.9646^{+0.0045}_{-0.0045}$	$0.9669^{+0.0039}_{-0.0039}$	$0.967^{+0.0038}_{-0.004}$
M_{tot}	< 0.26	< 0.12	< 0.16
N_{eff}	fixed 3.046		
Ω_m	$0.3188^{+0.0091}_{-0.016}$	$0.3078^{+0.0060}_{-0.0071}$	$0.3079^{+0.0065}_{-0.0085}$
H_0	$67.14^{+1.3}_{-0.72}$	$67.97^{+0.56}_{-0.49}$	$67.95^{+0.66}_{-0.52}$
σ_8	$0.8053^{+0.019}_{-0.0091}$	$0.8135^{+0.01}_{-0.0073}$	$0.8087^{+0.012}_{-0.0072}$

Ivanov+ 2020 Boss DR12

- The addition of the BAO breaks the degeneracy between h and the other cosmological parameters, including M_ν (they are anti-correlated in the CMB).
- FS (with unreconstructed BAO peak) also carries information on clustering amplitude, which is somewhat lower than CMB, which pulls the M_ν upper limit up.
- Information carried by BAO and FS is different but, in Boss, their constraining power is similar. FS measurements will become more powerful in next-generation experiments.

Constraints from LSS. What Next

Chudaykin & Ivanov 2020

Real space (No RSD, No AP)

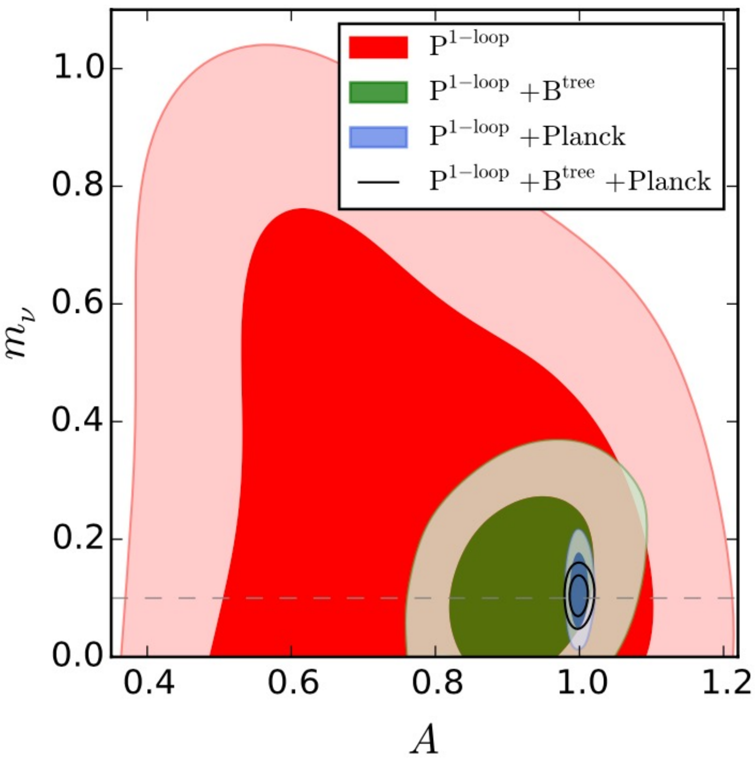

Redshift space (+ RSD, + AP)

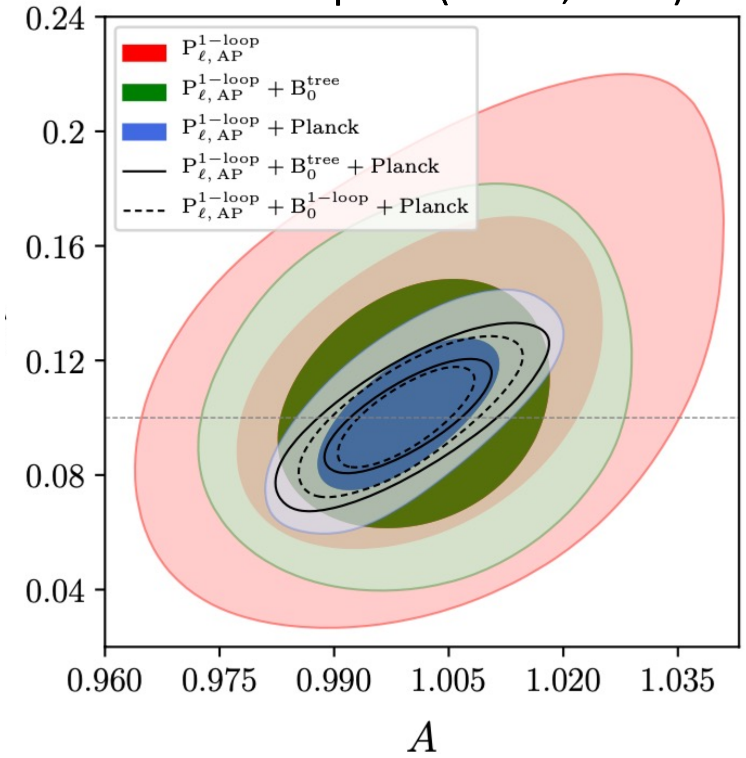

1. Benefit from adding 3-point statistics: remove bias parameters' degeneracy.
2. Benefit from RSD: adding z-dependent multipoles removes A ; b_1 degeneracy.
3. Benefit from AP: h-independent constraints sensitive to Ω_M. It improves M_ν constraints.

Next-generation surveys like Euclid could reach a 0.02 eV sensitivity

(for neutrinos with mass 0.06 eV)